AFRL-AFOSR-UK-TR-2023-0029

Giga Electron Volt Scale High-Repetition-Rate Plasma Accelerator

Simon Hooker
THE UNIVERSITY OF OXFORD
UNIVERSITY OFFICES
OXFORD, ,
GB

11/17/2022
Final Technical Report

Air Force Research Laboratory
Air Force Office of Scientific Research
European Office of Aerospace Research and Development
Unit 4515 Box 14, APO AE 09421

REPORT DOCUMENTATION PAGE

PLEASE DO NOT RETURN YOUR FORM TO THE ABOVE ORGANIZATION.

1. REPORT DATE	2. REPORT TYPE	3. DATES COVERED	
20221117	Final	START DATE 20180815	END DATE 20220814

4. TITLE AND SUBTITLE
Giga Electron Volt Scale High-Repetition-Rate Plasma Accelerator

5a. CONTRACT NUMBER	5b. GRANT NUMBER	5c. PROGRAM ELEMENT NUMBER
	FA9550-18-1-7005	61102F
5d. PROJECT NUMBER	**5e. TASK NUMBER**	**5f. WORK UNIT NUMBER**

6. AUTHOR(S)
Simon Hooker

7. PERFORMING ORGANIZATION NAME(S) AND ADDRESS(ES)
THE UNIVERSITY OF OXFORD
UNIVERSITY OFFICES
OXFORD
GB

8. PERFORMING ORGANIZATION REPORT NUMBER

9. SPONSORING/MONITORING AGENCY NAME(S) AND ADDRESS(ES)	10. SPONSOR/MONITOR'S ACRONYM(S)	11. SPONSOR/MONITOR'S REPORT NUMBER(S)
EOARD UNIT 4515 APO AE 09421-4515	AFRL/AFOSR IOE	AFRL-AFOSR-UK-TR-2023-0029

12. DISTRIBUTION/AVAILABILITY STATEMENT
A Distribution Unlimited: PB Public Release

13. SUPPLEMENTARY NOTES

14. ABSTRACT
This report describes work undertaken between 15th August 2018 and 14th August 2022 under grant number FA9550-18-7005. Two topics relating to the development of laser-driven plasma accelerators were studied. The first of these --- the multi-pulse laser wakefield accelerator (MP-LWFA) --- provides a means to increase the pulse repetition rate of laser wakefield accelerators, which is currently at least two orders of magnitude too low for the most interesting applications. We demonstrate experimentally two key steps necessary for development of MP-LWFAs. First we show that trains of laser pulses, with a total energy in the joule range, can be guided over long (100 mm) plasma channels. Second, we show that these guided pulse trains can resonantly excite a plasma wave when the plasma density is tuned so that the spacing of the laser pulses matches the natural oscillation period of the plasma. In addition to this experimental work we describe a new concept --- the plasmamodulated plasma accelerator (P-MoPA) --- for converting a single long (picosecond duration) laser pulse into a train of short laser pulses suitable for driving a MP-LWFA. We also report on experimental and theoretical work that demonstrates that motion of the plasma ions will not cause deleterious effects in practical MP-LWFAs. The second topic we investigate is the development of methods for extending the length of the plasma accelerator by guiding the driving

15. SUBJECT TERMS

16. SECURITY CLASSIFICATION OF:			17. LIMITATION OF ABSTRACT	18. NUMBER OF PAGES
a. REPORT U	b. ABSTRACT U	c. THIS PAGE U	SAR	26

19a. NAME OF RESPONSIBLE PERSON	19b. PHONE NUMBER *(Include area code)*
ANDREW GREENWOOD	314 235 6037

Grant number: FA9550-18-1-7005
Research title: GeV-Scale, High-Repetition-Rate Plasma Accelerators
PI: Simon M. Hooker
Period: 15th August 2018 to 14th August 2022

Contents

List of Figures

Abstract

This report describes work undertaken between 15th August 2018 and 14th August 2022 under grant number FA9550-18-7005.

Two topics relating to the development of laser-driven plasma accelerators were studied. The first of these — the multi-pulse laser wakefield accelerator (MP-LWFA) — provides a means to increase the pulse repetition rate of laser wakefield accelerators, which is currently at least two orders of magnitude too low for the most interesting applications. We demonstrate experimentally two key steps necessary for development of MP-LWFAs. First we show that trains of laser pulses, with a total energy in the joule range, can be guided over long (100 mm) plasma channels. Second, we show that these guided pulse trains can resonantly excite a plasma wave when the plasma density is tuned so that the spacing of the laser pulses matches the natural oscillation period of the plasma. In addition to this experimental work we describe a new concept — the plasma-modulated plasma accelerator (P-MoPA) — for converting a single long (picosecond duration) laser pulse into a train of short laser pulses suitable for driving a MP-LWFA. We also report on experimental and theoretical work that demonstrates that motion of the plasma ions will not cause deleterious effects in practical MP-LWFAs.

The second topic we investigate is the development of methods for extending the length of the plasma accelerator by guiding the driving laser pulse(s) through the plasma. We describe a new method for creating plasma channels — hydrodynamic optical-field-ionized (HOFI) plasma channels — and demonstrate experimentally that they can guide intense laser pulses over more than 100 mm of low density plasma. Further experimental and numerical work shows that the propagation loss of a HOFI channel can be reduced very considerably by conditioning it with an additional laser pulse guided by the HOFI channel. These conditioned HOFI (CHOFI) channels are shown to have power attenuation lengths of order 20 m. Experiments on electron acceleration in HOFI channels demonstrate acceleration to an energy of ~ 1 GeV. We also demonstrate experimentally that HOFI channels can be operated at kilohertz repetition rates for an extended period. Together these results indicate that HOFI and CHOFI channels could provide robust, metre-scale, multi-GeV plasma accelerator stages operating at repetition rates in the kilohertz range.

The work undertaken in this programme on MP-LWFAs and HOFI channels opens a route to achieving compact, GeV-scale plasma accelerators operating at kilohertz repetition rates.

1 Accomplishments

1.1 Introduction

Laser-driven plasma accelerators generate electron beams with energies comparable to those used in today's 3rd- and 4th-generation light sources, but in an accelerator stage only a few centimetres long. As such they have the potential to drive a new generation of compact sources of particles and radiation.

This programme aimed to address two key challenges which must be overcome before plasma accelerators can realize the full promise. First, the Ti:sapphire lasers used today typically operate at repetition rates of order 1 Hz and have wall-plug efficiencies below 0.1%; both these parameters are at least two orders of magnitude too low for the high-mean-power plasma accelerators that would be required to drive compact light sources or new types of particle collider. Second, in order to maintain acceleration over a long distance — and hence to achieve a large energy gain — it is necessary to overcome diffraction of the driving laser pulse.

In the sections below we describe in turn the extent to which we were able to make progress in meeting these two challenges.

1.2 MP-LWFAs

To address the first of these challenges we proposed to investigate the prospect of driving the plasma wakefield with a train of lower energy laser pulses, which could be provided by novel, efficient laser technologies — an approach known as the multi-pulse laser wakefield accelerator (MP-LWFA). In our proposal we identified the following objectives for this part of the programme:

1. To investigate the potential for chirped pulse trains to drive plasma wakefields beyond the limits set by relativistic detuning.
2. To investigate the use of autoresonance to increase the tolerance to plasma density variations
3. To explore the potential for post-acceleration recovery of unused wakefield energy by trailing laser pulses
4. To establish a MP-LWFA pulse train design based on realistic near-term laser parameters

We pursued these objectives through a combination of numerical simulations, primarily with particle-in-cell (PIC) codes, experiments in our laboratories in Oxford, and experiments at national laser facilities. Most of the objectives were met in full.

Building on work started prior to this programme, we employed numerical analysis and PIC simulations to explore the potential for non-uniformly-spaced pulse trains to drive larger-amplitude plasma waves [Objective (1)], and to explore the possibility of using autoresonance to increase the tolerance of MP-LWFAs to variations in the plasma density [Objective (2)]. This work showed that chirped pulse trains could be used to overcome the effects of relativistic detuning, and that autoresonance could be used to mitigate the effects of non-uniformities in the plasma density. This work is described in detail in Dr Chris Arran's D. Phil. thesis.[1]

We developed an experiment to test the concepts behind Objectives (1) and (3), and were awarded time (CLF experiment 18110004) to undertake this on the Astra-Gemini TA3 laser at the Central Laser Facility (CLF), Rutherford Appleton Laboratory (RAL). Unfortunately, as explained in §3.1, a large number of technical problems with the CLF lasers meant that only one of the original objectives of the experiment could be met. We applied for, and were awarded, additional beam time to complete these experiments, but delays — primarily arising from the pandemic — meant that it was more than three years before we could return to this experiment. Given this long delay we revised the objectives of this experiment to concentrate on demonstrating two key milestones for MP-LWFAs. This work was very successful. First we showed that high-energy (joule-scale) trains of laser pulses could be guided in HOFI plasma channels more than 100 mm long. Second, we showed that the pulse trains could excite plasma waves when the density of the channel was tuned into resonance with the pulse train. A paper describing this work is being prepared for publication.

One of the original objectives of Experiment 18110004 was to measure the time taken for the plasma wave to decay. We were able to complete these measurements for plasma waves driven by single laser pulses. This work has been described in detail in Dr Jakob Jonnerby's D. Phil. thesis[2] and is summarized in §4.1.3. A journal paper on these experiments is being prepared for publication.

In addition we undertook a detailed numerical study of the effects of ion motion on the plasma wakefield. In this work, we identified the modulational instability as being responsible for the decay of the wakefield amplitude. A journal paper on this work has been submitted for publication;[3] further details are available in Dr Alexander von Boetticher's D. Phil. thesis.[4]

Our most significant achievement in this section of the programme was the development of a new concept for generating the driving pulse train required in a MP-LWFA [Objective 4]. Unlike other methods, this requires only a single high-energy laser pulse. This is of very great interest since lasers have recently been developed that can generate the required laser pulse energy (joule-scale) with high efficiency, and at high pulse repetition rates (kilohertz range), but which generate pulses that are too long to drive a plasma wave directly. This work was published[5] in *Physical Review Letters*, and we have applied for a patent to protect the associated IP.

In the new scheme – which we call the plasma-modulated plasma accelerator (P-MoPA) — a high-energy, picosecond-duration laser pulse is spectrally modulated by the low amplitude plasma wave driven by a low-energy, short laser pulse. As explained in detail in §4.1.1, the spectral modulation can be converted to a temporal one, yielding a pulse train suitable for driving a MP-LWFA. Our 2D PIC simulations show that currently available thin-disk lasers could be used to drive a P-MoPA generating GeV-scale electron bunches at repetition rates in the kilohertz range.[5]

1.3 HOFI plasma channels

To address the second challenge, we proposed to investigate a new type of plasma channel (i.e. a structure analogous to an optical fibre, but made from plasma) which was capable of guiding very intense laser pulses over many centimetres of plasma, and which had the potential to operate at high pulse repetition rates for extended periods. In particular we proposed to investigate the hydrodynamic optical-field-ionized (HOFI) plasma channel invented by the Oxford group. This part of the programme had the following objectives:

1. To investigate how the channel properties depend on those of the channel-forming pulse and the target gas.
2. Demonstration of generation of HOFI plasma channels of length > 100 mm with on-axis density below $n_{e0}(0) = 1 \times 10^{18}\,\mathrm{cm}^{-3}$.
3. To demonstrate guiding of high-intensity laser pulses through HOFI plasma channels.
4. To develop optical designs for generating HOFI plasma channels suitable for laser-plasma accelerators.

This work was undertaken through experiments in Oxford, and at national laser facilities, hydrodynamic simulations of the channel formation, and PIC simulations of the propagation of electron acceleration by intense laser pulses guided by plasma channels.

As described in detail in §4.2.2, we demonstrated[6] the generation of 100 mm long HOFI plasma channels with on-axis densities measured interferometrically to be as low as $n_{e0}(0) = (1 \pm 0.3) \times 10^{17}\,\mathrm{cm}^{-3}$ [Objective (1)]. We also demonstrated[6] that laser pulses with a peak intensity of $6 \times 10^{17}\,\mathrm{W\,cm}^{-2}$ could be guided through 100 mm long HOFI plasma channels [Objective (2)]. Further, we showed[7] that metre-scale, low-density plasma channels could be generated by using an additional laser pulse, or the leading edge of the guided pulse, to ionize the collar of gas surrounding the HOFI plasma channel. These conditioned HOFI (CHOFI) channels were shown to have power attenuation lengths as long as 20 m.

We have made excellent progress towards the development of designs of (C)HOFI channels for plasma accelerator stages [Objective (4)]. One of the very attractive features of (C)HOFI channels is that they are free-standing, and hence are in principle capable of operation at high pulse repetition rates for extended periods. In recent work, described further in §4, we demonstrated experimentally that the properties of two HOFI channels generated 1 ms apart are essentially the same, and hence that operation at kHz repetition rates is in principle possible. We also demonstrated that HOFI channels can be generated at a mean repetition rate of 0.4 kHz for a period of 6.5 hours without degradation of the channel properties.

In new experiments undertaken with the Astra-Gemini TA3 laser, described in §4.2.5, we have successfully accelerated electrons to an energy of 1 GeV in a CHOFI plasma channel. We also demonstrated a novel method for controlling the injection of electrons into plasma waves driving within (C)HOFI channels. This work will be submitted for publication in the next few months.

We were able to make some progress towards Objective (1), but this was slower than anticipated since construction of new, radiation-shielded high-power laser laboratories in Oxford was delayed significanlty, as explained in §3.1. We plan to return to this work in the next few months.

1.4 Dissemination

To date our results have been published in several journal papers,[3,5–10] with further papers in preparation, as well as being described in four D. Phil. theses.[1,2,4,11] These publications are available from the Oxford Research Archive (`https://ora.ox.ac.uk`).

In addition we presented these results at the following international conferences and workshops:

- January 2018: Laser Electron Acceleration at Kilohertz (LEAK) Workshop, ELI Beamlines, Prague, Czech Republic
- March 2019: ALEGRO Workshop, CERN
- August 2019: SPIE Optics and Optoelectronics Symposium, Prague, Czech Republic
- September 2019: European Advanced Accelerator Concepts Workshop, Elba, Italy
- April 2021: SPIE Optics and Optoelectronics Symposium, Prague, Czech Republic
- September 2022: EuroNNAc Special Topics Workshop, Elba, Italy
- November 2022: Advanced Accelerator Concepts Workshop, Long Island, USA

2 Impacts

Our work on MP-LWFAs and HOFI plasma channels has received considerable attention from international groups seeking to develop the next generation of particle colliders. For example, our work on both these topics has been cited in the new European Strategy for Particle Physics - Accelerator R& D Roadmap.[12] Our work on HOFI channels has also been cited in White Papers for an equivalent roadmap being developed under the "Snowmass" process in the USA.[13]

The HOFI plasma channels developed in this programme are already being adopted by other groups working in the field. For example:

1. We are collaborating with Prof. Stefan Karsch of Ludwig Maximilians Universität, Munich on deploying HOFI channels in his GeV-scale plasma accelerator experiments.
2. We are collaborating with the group at DESY on improving hydrodynamic models of the formation of HOFI plasma channels.
3. Prof. M. Downer's group at University of Texas has proposed experiments on controlling electron injection into plasma wakefields driven in HOFI channels.

The P-MoPA concept developed during this programme has attracted interest. We have established the kilohertz Plasma Accelerator Consortium (kPAC) to develop this scheme further and to demonstrate the key steps involved. At present the other members of kPAC are LMU, CLF, and Trumpf Scientific Lasers.

3 Changes

3.1 Problems or delays

We experienced some very significant delays in our programme of experiments at the CLF. These were caused by technical problems with the laser, and the restrictions arising from the response to the Covid pandemic. We summarize these delays below:

- Experiment 18110004 with the CLF's Astra-Gemini TA3 laser was undertaken between 24th September and 16th November 2018. Severe technical problems meant that it was only possible to complete one of the five objectives.
- We applied for, and were awarded, additional access to the Gemini laser (Experiment 19210001) to complete the objectives of Experiment 18110004. This new experiment was initially scheduled for August 2020, but was later rescheduled for January 2021 so that it could follow a new experiment on HOFI plasma channels (Experiment 20110003), which was scheduled for December 2020.
- Experiments 19210001 and 20110003 were then both postponed to 2021 as a result of the COVID-19 pandemic. Both experiments were undertaken during an extended period of beam access between 4th October 2021 and 28th January 2022.

The delay in completing Experiment 18110004 was more than three years. Given this we revised the objectives of this experiment.

Shortly before the start of this project the university approved an investment of £1.45M for the construction of new, fully radiation shielded and temperature-stabilized high-power laser laboratories for use by the PI. In addition, funding from two Science and Technology Facilities Council (STFC) Capital Equipment grants, plus investment by Oxford Physics, provided £640k to upgrade our Ti:sapphire laser system to incorporate adaptive wavefront control and beam pointing stabilization, and to increase the peak power to 15 TW (600mJ (post compressor), 40 fs, 10Hz).

Construction of the new laboratories was completed in November 2019, and the upgraded laser was installed and commissioned in March 2020. Unfortunately, significant delays were caused by pandemic-related restrictions. We also experienced very significant problems with the supplier of the laser and radiation interlock system, which meant that we had to commission and install a second interlock system. As a consequence the laser system only became available to the project in its last few months, and hence very little of the work originally envisaged to be undertaken in Oxford could be completed.

It is pleasing to report that the laser is now operational and was very recently used to demonstrate laser-acceleration of electrons for the first time in Oxford.

Given these problems, we are very grateful that AFOSR agreed to extend this project for 12 months.

3.2 Expenditure impacts

During the period of this grant we received considerable funding (£2.03M) from the Engineering and Physical Sciences Research Council (EPSRC) for a four-year project on "All-Optical Plasma Channels and Electron Injection with Spatio-temporal Control." The overlap with the AFOSR, staff changes, and uncertainties introduced by the pandemic, meant that we were not able to spend all the AFOSR budget allocated to staff. With the agreement of the Program Officer, Dr Nathaniel P. Lockwood, we therefore used some of the staff budget to purchase items to assist with commissioning and completing the new high-power laser laboratories in Oxford.

4 Technical updates

4.1 Multi-pulse laser wakefield accelerators

Laser-driven plasma accelerators can accelerate few-femtosecond duration electron bunches to multi-GeV energies in accelerator stages only a few centimetres long. They therefore offer the potential to drive compact sources of energetic particles and radiation, including free-electron lasers. However, the lasers used today to drive plasma accelerators operate at low pulse-repetition-rates ($f_{\rm rep} \lesssim 10\,$Hz). They also have very low wall-plug efficiency ($< 0.1\%$), which is two orders of magnitude too low to drive future generations of particle collider.

In the multi-pulse laser wakefield accelerator (MP-LWFA), the plasma wave is driven by a train of low-energy laser pulses, rather than by a single high-energy pulse. This opens plasma accelerators to new laser technologies that can generate the required laser pulse energy — at high pulse repetition rates ($f_{\rm rep} \gtrsim 1\,$kHz), and with high wall-plug efficiency ($\gtrsim 10\%$) — but which produce pulses that are too long to drive the plasma wave directly.

In the following sections we describe our progress in developing MP-LWFAs.

4.1.1 Plasma-modulated plasma accelerators (P-MoPAs)

During this programme we developed a new method for generating the pulse train required to drive a MP-LWFA. Unlike other methods,[14] which are related to the beat-wave principle, this requires only a single high-energy laser pulse. It therefore offers the possibility of building on the recent impressive progress in the development of thin-disk laser technology. For example, thin-disk lasers have optical-to-optical efficiencies exceeding 50% and have recently generated pulse energies of $\sim 1\,$J at $f_{\rm rep} = 1\,$kHz.[15–17] However, their long (picosecond) pulse duration makes them unsuitable for driving LPAs directly. We note that spectral broadening in gases has been shown[18–20] to reduce the duration of thin-disk laser pulses, but sub-100 fs pulses with the energy required to drive high-energy LPAs have yet to be demonstrated.

In the new scheme, a high-energy, picosecond-duration laser pulse is spectrally modulated by the low amplitude plasma wave driven by a low-energy, short laser pulse (which can be generated at high repetition rates). As we explain below, the spectral modulation can be converted to a temporal one, yielding a pulse train suitable for driving a MP-LWFA. We have named this approach the plasma-modulated plasma accelerator (P-MoPA). This work was published[5] in *Physical Review Letters*, and we have applied for a patent to protect the associated IP.

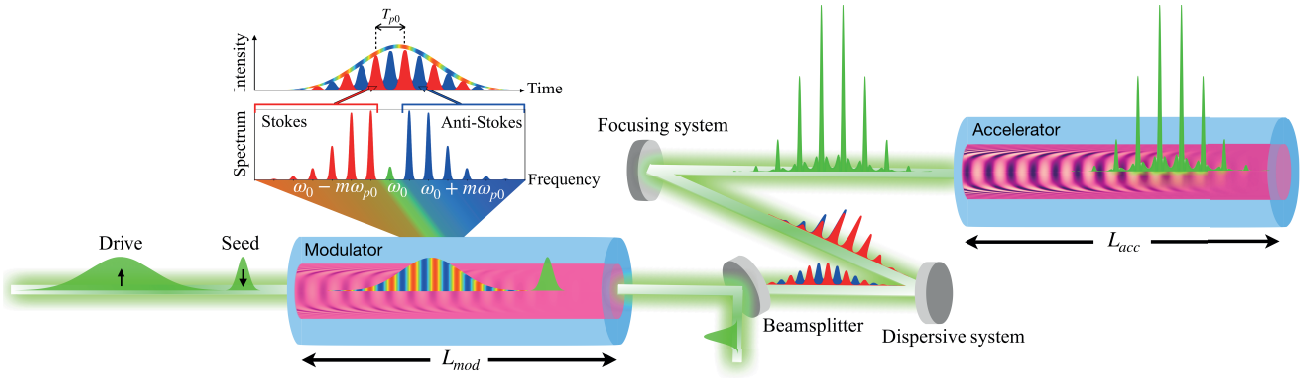

Figure 1: Schematic diagram of a plasma-modulated plasma accelerator. A long, high-energy, drive laser pulse is phase-modulated in the modulator stage by its interaction with the plasma wave driven by a short, low-energy seed pulse. The modulation generates sidebands at $\omega_0 + m\omega_{\rm p0}$, although the temporal intensity profile of the drive pulse remains smooth. After leaving the modulator stage, the seed pulse is removed by a polarizing beam-splitter, and the drive pulse is passed through (or reflected from) a dispersive optical system which removes the relative spectral phase of the sidebands, to form a train of short pulses spaced by $T_{\rm p0} = 2\pi/\omega_{\rm p0}$. This pulse train is focused into an accelerator stage, which comprises a plasma channel with the same on-axis density as that of the modulator stage. The pulse train resonantly excites a strong plasma wave that can be used for particle acceleration.

As shown in Fig. 1, our approach has three stages. In the first, the modulator stage, a short ($\tau_{\rm seed} \lesssim T_{\rm p0}/2$), low energy seed pulse and a long ($\tau_{\rm drive} \gg T_{\rm p0}$), high-energy driving laser pulse are focused into a plasma waveguide. Here $T_{\rm p0} = 2\pi/\omega_{\rm p0}$ refers to the plasma period on-axis. The seed pulse drives a low amplitude plasma wave which periodically modulates the temporal phase of the drive pulse, and hence generates frequency sidebands at $\omega_0 + m\omega_{\rm p0}$. If isolated, the red- ($m < 0$) and blue-shifted ($m > 0$) sidebands would form a pair of *temporal* pulse trains separated by $T_{\rm p0}/2$, but when both sets of sidebands are present the temporal profile of the drive pulse remains smooth.

In the second stage, after removal of the seed pulse, the spectrally-modulated drive pulse is converted into a temporally-modulated train of short pulses, separated by $T_{\rm p0}$, by introducing a shift of $T_{\rm p0}/2$ between the red- and blue-shifted trains. This can be achieved by introducing a dispersive optical system with the correct group delay dispersion (GDD).

In the third (accelerator) stage, the pulse train is focused into a second plasma waveguide with the same axial density as the modulator, which resonantly excites a large-amplitude plasma wave for acceleration of externally injected electrons.

In order to gain insight into the modulation process, we developed a 1D analytic model. The drive pulse has a normalized vector potential, $a(z,t) = b(z,t)\exp\left[{\rm i}(k_0 z - \omega_0 t)\right]$, where ω_0 is the centre frequency of the pulse, and z is the coordinate along the propagation axis. After co-propagating a distance z with a linear plasma wave of density $n_e(z,t) = n_0 + \delta n\cos\left(k_{p0}z - \omega_{p0}t + \Delta\phi\right)$, the envelope of the pulse becomes,[21]

$$b(\zeta,\tau) \approx |b(\zeta,0)| \sum_{m=-\infty}^{\infty} {\rm i}^m J_m(-\beta)\exp\left[{\rm i}m\left(\omega_{p0}\tau + \Delta\phi'\right)\right]. \qquad (1)$$

Here $\zeta = z - v_g t$, where v_g is the group velocity of the driver, $\tau = t$, $\beta = (1/2)(\omega_{p0}^2/\omega_0)(\delta n/n_0)(z/v_g)$, and $\Delta\phi' = -(\Delta\phi + \omega_{p0}z/v_p)$, where v_p is the phase velocity of the plasma wave. The generation of sidebands at $\omega_0 + m\omega_{p0}$ is immediately apparent. In the temporal domain, the red- and blue-shifted sidebands each form trains of pulses separated by $T_{\rm p0}$, with a relative shift between the two trains of $T_{\rm p0}/2$.

We also performed high-resolution 2D PIC simulations with the EPOCH code[22] in order to understand the operation of this scheme in detail. The parameters of the drive and seed laser pulses were chosen to be similar to those recently demonstrated for thin-disk lasers operating at $f_{\rm rep} \gtrsim 1\,$kHz at a wavelength of $\lambda_0 = 1030\,$nm. Both pulses were assumed to be bi-Gaussian, with a drive (seed) energy of $E_p^{\rm drive} = 600\,$mJ ($E_p^{\rm seed} = 50\,$mJ) and a full-width at half maximum pulse duration of $\tau_{\rm drive} = 1\,$ps ($\tau_{\rm seed} = 40\,$fs). The pulses were separated by 1.7 ps.

The plasma parameters of the modulator and accelerator stages were identical. For radii $r < r_0 = 1.2w_M$, the electron density was $n_{ch}(r) = n_{e0} + (1/\pi r_e w_M^2)(r/w_M)^\alpha$, where $n_{e0} \equiv n_e(0) = 2.5\times10^{17}\,{\rm cm}^{-3}$,

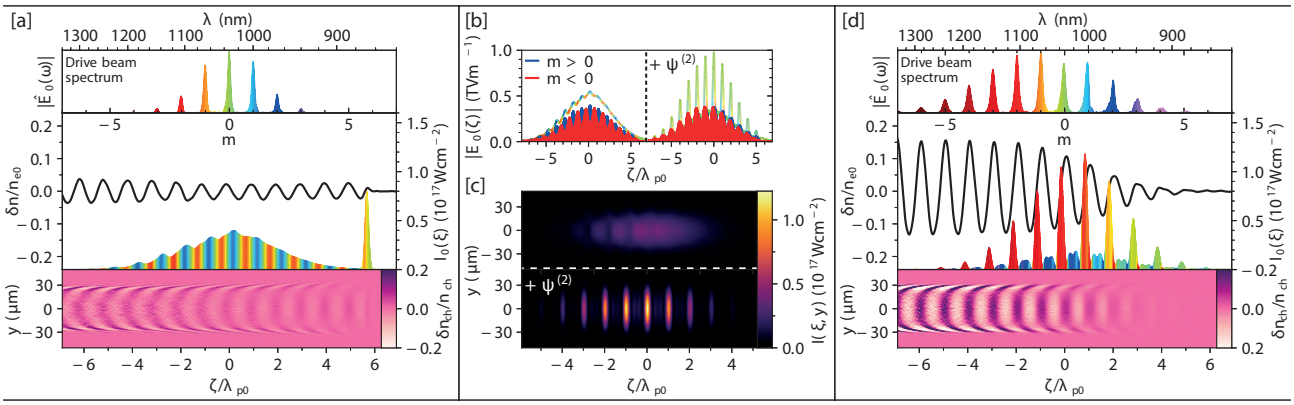

Figure 2: Numerical simulations of a P-MoPA. (a) PIC simulations of the modulator stage, with results shown for the end of the modulator ($z = 120\,\mathrm{mm}$). The top panel shows the on-axis spectral intensity of the drive pulse, plotted against a frequency scale $m = (\omega - \omega_0)/\omega_{\mathrm{p0}}$. The middle panel shows the longitudinal intensity profiles of the seed and driver pulses and the relative amplitude of the plasma wave on axis ($y = 0$). The bottom panel shows, for $z = 120\,\mathrm{mm}$, a 2D plot of the electron density relative to the channel profile $\delta n_{ch}/n_{ch} = (n_e - n_{ch})/n_{ch}$. The shading of the longitudinal profiles indicates the local effective frequency $-\mathrm{d}\phi/\mathrm{d}t$, where ϕ is the temporal phase, using the same color scale as the top panel. (b) The modulus of the on-axis electric field of the drive pulse together with the red- and blue-shifted components before and after application of a quadratic spectral phase $\psi^{(2)} = -1480\,\mathrm{fs}^2$. (c) The corresponding 2D intensity profiles. (d) The same plots as in (a) but at a distance $z = 50\,\mathrm{mm}$ into the accelerator stage.

and $w_M = 30\,\mu$m is approximately the spot size of the lowest-order channel mode. For $r > 1.2w_M$, $n_e(r) = n_e(r_0)$ for $\Delta r = 10\,\mu$m, before decreasing linearly to zero in the same distance. The parameter $\alpha = 10$, and hence the channels were steep-sided, with finite losses. The drive and seed pulses were focused to a spot-size $w_0 = w_M = 30\,\mu$m at the entrance to the modulator channel.

Figure 2(a) shows that the seed pulse drives a plasma wave of amplitude $\delta n/n_{e0} \approx 2\%$ on axis, which generates side-bands on the drive pulse at $\omega_0 + m\omega_{\mathrm{p0}}$, although its temporal profile remains smooth. Figures 2(b,c) show, after the modulator, the on-axis electric field (b) and temporal intensity profile (c) of the drive pulse, before and after the application of a quadratic spectral phase with a group delay dispersion (GDD) of $\psi^{(2)} = -1480\,\mathrm{fs}^2$, which was determined numerically to produce the highest-intensity pulse train. It is evident that the dispersion converts the phase-modulated, but temporally-smooth, drive pulse into a train of short pulses separated by $T_{\mathrm{p0}} = 220\,\mathrm{fs}$.

Figure 2(d) shows the calculated drive pulse train, and the plasma wake, after 50 mm propagation in the accelerator stage. The pulse train resonantly excites a strong plasma wave with $\delta n/n_e \approx 15\%$ over the whole length of the accelerator. The spectrum of the driver is further modulated by this plasma wave, leading to the formation of additional sidebands through electromagnetic cascading; it is also red-shifted, the shift increasing towards the back of the pulse train, where the wake amplitude is higher.

In Fig. 3 we demonstrate that the scheme can be scaled to higher drive pulse energies, and hence higher acceleration gradients, whilst ensuring that the modulator operates in a well-controlled, linear regime. For these simulations the parameters of the accelerator stage, and the axial density of the modulator stage, were the same as in Fig. 2. However, the matched spot size of the modulator was increased to 50 µm in order to allow the seed and drive pulse energies to be increased to 140 mJ and 1.7 J whilst keeping their peak intensities the same as in Fig. 2. Figure 3(a) shows clearly that a quasi-linear wakefield, with an amplitude considerably larger than that of Fig. 2, can be driven over the entire length of the 100mm acceleration stage.

To demonstrate particle acceleration, a 1 pC electron bunch of energy 35 MeV, 5 fs root-mean-square duration, and 4 μm transverse width was injected into the focusing phase of the wakefield, at the position of peak acceleration. Figure 3(c) shows the evolution with z of the normalized energy spectrum $\hat{Q}_e(W_e, z)$ of this bunch, where W_e is the electron energy. It can be seen that the bunch maintains a relatively narrow energy spectrum up to $z \approx 50\,\mathrm{mm}$, at which point the mean energy is $\sim 500\,\mathrm{MeV}$. At larger z, dephasing causes the energy spectrum to broaden. The mean electron energy at the end of the accelerator stage is 0.65 GeV. The laser-plasma energy transfer in the accelerator stage is found to be 9%.

Our results demonstrate the operation of this scheme, but further work will be required to fully explore its potential. For example, it is likely that the energy transfer efficiency could be increased, and the properties

of the accelerated bunch improved, by optimizing the parameters of the drive laser and plasma channel, and the beam loading of the plasma wakefield.

We note that the key components required to realize this new approach have all recently been demonstrated, and, in principle, all are capable of multi-kilohertz operation. In particular, we have developed meter-scale, low-loss, all-optical plasma waveguides capable of kHz repetition rates, as described in §4.2. Further, 100 mJ-scale, sub-50 fs seed laser pulses, and joule-level, few-picosecond, 1030 nm drive laser pulses have been demonstrated.[15,17]

4.1.2 Resonant excitation of plasma waves in HOFI channels

We recently completed experiments (Experiment no. 19210001) undertaken with the Astra-Gemini TA3 laser facility at CLF which were aimed at demonstrating some of the key concepts of a MP-LWFA stage. This experiment was a follow-on experiment to Gemini experiment no. 18110004, performed in September 2018, during which significant technical problems were encountered (see §3.1). The experiment was undertaken in December 2021 and January 2022.

The revised objectives of this experiment were to demonstrate that: (i) a high-energy laser pulse train could be guided over an extended distance in a HOFI plasma channel; and (ii) that the pulse train could resonantly excite a plasma wave.

For this work, the pulse train was generated from a single, frequency-chirped laser pulse from the Gemini Ti:sapphire laser system. The frequency chirp was obtained by only partially compressing the laser pulse from the final Ti:sapphire amplifier; this pulse was negatively-chirped (i.e. the frequency of the pulse decreased towards the back of the pulse), and it had a full-width at half maximum (FWHM) duration of approximately 1 ps. This chirped pulse was converted to a train of $N \approx 10$ short pulses by passing it through a Michelson interferometer, which acted as a spectral filter.[23] (The spectral — and hence temporal — modulation of the chirped pulse is evident in Fig. 5(a).) The temporal profile of the pulse train was deduced from single-shot autocorrelation measurements, combined with measurements of the spectrum of the pulse train. The total energy of the pulse train was 2.5 J.

The HOFI plasma channel was generated by a short ($\sim$ 50 fs) pulse, of $\sim$ 100 mJ energy, that was derived from the other arm of the Gemini laser. This pulse was focused by an axicon lens into a 110 mm long, H_2-filled gas cell, to form an initial plasma column 3.5 ns before the arrival of the pulse train. The pulse train was focused to the entrance of the HOFI channel by an off-axis paraboloid, used at $f/40$.

Figure 4 shows the results of a preliminary analysis of experiments to demonstrate that the pulse train could be guided by the HOFI channel. It is clear from Fig. 4(a) and (b) that high-quality guiding over 110 mm was indeed achieved. Fig. 4(c) shows the variation of the spot size of the transmitted pulse train as a function of the on-axis density of the HOFI channel. It is evident that the spot size of the transmitted pulse train remained close to that of the input pulse train over a wide range of on-axis density.

In order to demonstrate that a plasma wave could be driven by the guided pulse train, we measured the spectrum of the transmitted pulse train as a function of the on-axis density of the plasma channel. Figure 5(a) compares the spectrum of the pulse train at the entrance and exit of a 110 mm long HOFI plasma channel for two different on-axis plasma densities. For these experiments, resonant excitation was expected to occur at an on-axis density of $n_{e0} \approx 5.0 \times 10^{17}\,\mathrm{cm}^{-3}$. It is clear that for this on-axis density the spectrum of the transmitted pulse train was broadened very significantly to longer wavelengths. This large red-shift is consistent with the pulse train driving a large-amplitude plasma wave. In contrast, away from the resonant density, the spectral modulation of the pulse train is small, indicating that any plasma wave driven by the pulse train had a low amplitude. Further evidence that the density-dependent red-shift

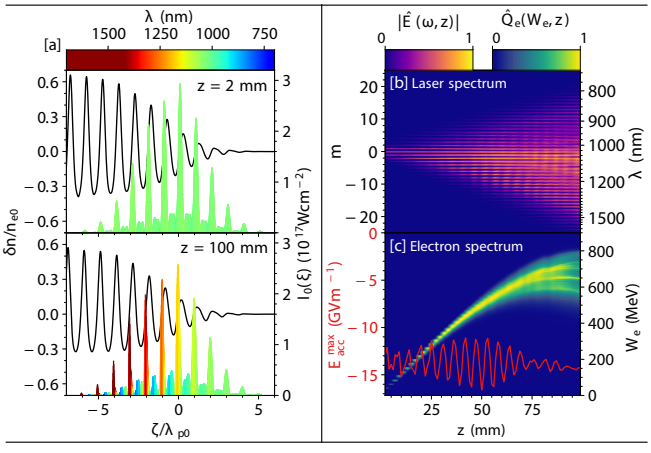

Figure 3: Performance of a scaled accelerator with seed and drive pulse energies increased to 140 mJ and 1.7 J respectively. (a) The on-axis longitudinal profiles of the laser intensity and the relative electron density $\delta n/n_0$ at $z = 2$ mm (top) and $z = 100$ mm (bottom) in the acceleration stage. The color scale shows the local laser wavelength. (b) Evolution of the normalized spectral intensity of the drive laser with propagation distance z in the acceleration stage. (c) Evolution of the normalized energy spectrum $\hat{Q}_e(W_e, z)$ of the injected electron bunch with z.

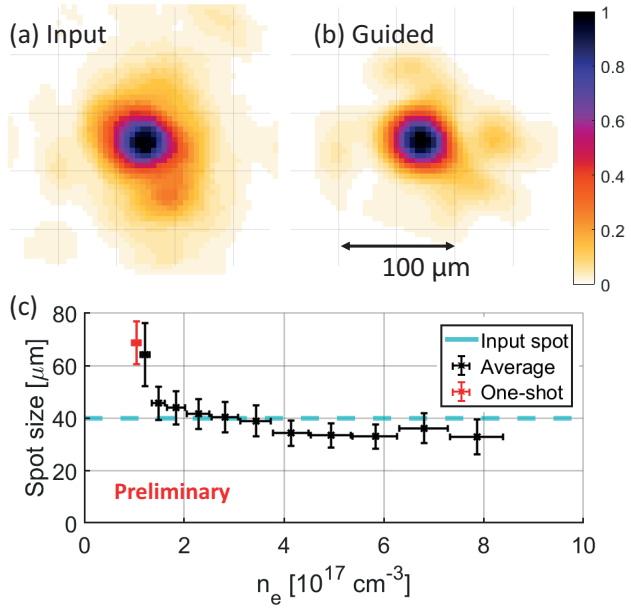

Figure 4: Preliminary analysis of experiments to demonstrate guiding of high-energy pulse trains in a HOFI channel. (a) The transverse fluence profile of the focused pulse train at the entrance to the HOFI channel. (b) The transverse fluence profile of the pulse train at the exit of the 110 mm long HOFI channel. (c) The deduced spot size of the transmitted beam as a function of the estimated on-axis density of the HOFI channel.

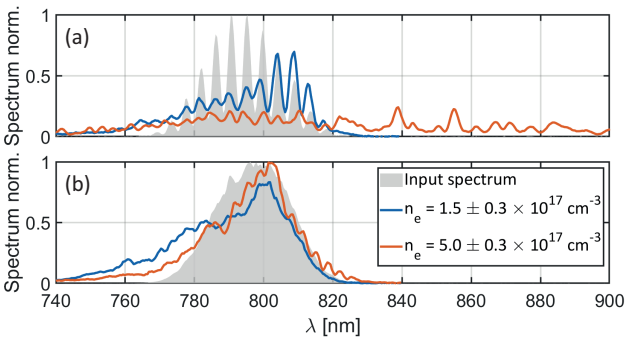

Figure 5: Preliminary analysis of experiments to demonstrate resonant excitation of plasma waves in a HOFI plasma channel. (a) Comparison of the spectrum of the pulse train at the entrance (grey) of a 110 mm long HOFI plasma channel with that at its exit for: (i) an on-axis density close to resonance, $n_{e0} = (5.0 \pm 0.3) \times 10^{17}\,\mathrm{cm}^{-3}$ (red); and (ii) away from resonance, $n_{e0} = (1.5 \pm 0.3) \times 10^{17}\,\mathrm{cm}^{-3}$ (blue). (b) As for (a), but for an unmodulated laser pulse of energy 2.5 J and duration 1 ps.

observed in Fig. 5(a) arises from resonant wakefield excitation is provide by Figure 5(b), which shows that a temporally-smooth laser pulse of approximately the same energy and total duration as the pulse train did not experience significant red-shifting at either plasma density. Further analysis will be undertaken to estimate the amplitude of the plasma wakefield driven in this experiment.

In summary, we successfully demonstrated two important steps for the realization of MP-LWFAs in general, and P-MoPAs in particular. First we showed that high-energy (joule-scale) trains of laser pulses could be guided in HOFI plasma channels more than 100 mm long. Second, we showed that the pulse trains could excite plasma waves when the density of the channel was tuned into resonance with the pulse train. A paper describing this work is being prepared for publication.

4.1.3 Studies of ion motion

In laser wakefield accelerators, the dynamics of the plasma ions are not important when the plasma wave is excited by a single, high-intensity pulse, owing to the small electron-to-ion mass ratio. However, motion of the ions can be important when the plasma wave is excited by pulse trains or modulated pulses that are long compared to the electron plasma period. As such, ion motion could be important in MP-LWFAs if the the pulse train is sufficiently long.

In order to provide further insight, we have undertaken particle-in-cell (PIC) studies of the onset of ion motion. PIC simulations of laser wakefields were performed with the relativistic PIC code `smilei`.[24] This work has been submitted for publication.[3]

The laser and plasma parameters assumed in the simulation were selected to obtain a wakefield with a density amplitude variation $\delta n_e/n_e$ on the order of 10%, corresponding to a large-amplitude regime where nonlinear relativistic effects are not strong. Full details of the parameters of the PIC simulations, and the laser and plasma conditions, are available in the paper submitted on this work.[3]

The wakefield excited by the laser pulse attains a maximum longitudinal electric field strength $E_x = 8.5$ GVm^{-1} on axis, wavelength $\lambda_{\mathrm{wake}} = \lambda_{\mathrm{pe}} \approx 2\pi c/\omega_{\mathrm{pe}} = 33.7$ μm and oscillates at the plasma frequency,

since $\omega_{k,\mathrm{pe}}^2 = \omega_{\mathrm{pe}}^2 + 3k^2 v_{\mathrm{th,e}}^2 \approx \omega_{\mathrm{pe}}^2$ for wavelengths $\lambda = 2\pi/k$ that are long compared to the Debye length, $\lambda_D = (\epsilon_0 k_{\mathrm{B}} T_{\mathrm{e}}/n_{\mathrm{e}} e^2)^{1/2} = 29.1$ nm. Here $v_{\mathrm{th,e}}$ denotes the electron thermal speed.

The longitudinal electric field of the wakefield is shown in Fig. 6(a), at $t = 0.32$ ps after the wakefield excitation. The on-axis longitudinal electric field strength is associated with a sinusoidal plasma density oscillation observed in the simulations of amplitude $\delta n_e/n_e = 0.09$. The transverse profile of the longitudinal electric field envelope is consistent with the laser pulse profile, with a transverse width $w_{\mathrm{fwhm}} = 45$ μm.

Within two picoseconds of the wakefield excitation, modulations of the longitudinal electric field and the ion density are observed to develop, with a characteristic length of 1.4 μm on-axis ($y = 0$) that is much smaller than the wakefield wavelength, $\lambda_{\mathrm{pe}} = 33.7$ μm. The modulations of the field and ion density are visible in Fig. 6(b) and 6(d), respectively, at $t = 2.56$ ps after wakefield excitation, and are shown magnified in the insets. The timescale for the growth of the modulations is thus on the order of the ion plasma period, $2\pi\omega_{\mathrm{pi}}^{-1} = 4.8$ ps. The wave number spectrum of the ion density is shown in Fig. 7 as a function of transverse position, indicating that modulations of the ion density grow fastest away from the axis, and that the wavelength of these modulations decreases with distance from the axis $y = 0$. The on-axis spectrum exhibits a peak at a wave number $k\lambda_D \approx 0.13$; a weaker, higher-order mode is seen to develop at $k\lambda_D \approx 0.26$. The modulations of the ion density are phenomenologically consistent with a modulational instability.[25,26]

Detailed analysis[3] of these results show that the growth rates, wave numbers, and the transverse profiles of the observed ion density modulations are found to be in good agreement with the one-dimensional dispersion relation of Sanmartin,[27] if the transverse dependence of the wakefield amplitude is accounted for. These results have implications for MP-LWFAs and the P-MoPA scheme described in §4.1.1. Since the modulational instability develops on a timescale comparable to the ion plasma period, it will become relevant for pulse trains with $N_{\mathrm{pulse}} \gtrsim (m_{\mathrm{i}}/m_{\mathrm{e}})^{1/2}/Z$, where m_{i} is the ion mass, and Z denotes the ion charge number. Indeed, in earlier work we showed that for long pulse trains with $N_{\mathrm{pulse}} \gg (m_{\mathrm{i}}/m_{\mathrm{e}})^{1/2}/Z$, the amplitude of the wakefield did not grow monotonically with pulse number,[14] indicating a loss of coherence of the electron oscillations. This earlier finding is explained by the simulations reported here. The non-monotonic dependence of the growth rate of the strong-field modulational instability (SFMI) on the electric field strength observed in our simulations[3] suggests that, in principle, the intensities of pulses in the driving train could be tuned to minimise the time for which the wakefield amplitude is such that the SFMI growth-rate is large. Alternatively, using a species with a high m_{i}/Z ratio, or heating the electronic component of the plasma could reduce the onset of the modulational instability, and allow longer pulse trains to be employed. Notwithstanding these points, although the effects of the modulational instability could be mitigated by these methods, they are unlikely to be necessary for MP-LWFAs or P-MoPAs since the number of pulses in the driving trains are expected to be $N_{\mathrm{pulse}} \sim 10 < (m_{\mathrm{i}}/m_{\mathrm{e}})^{1/2}$.

4.2 HOFI plasma channels

The development of long, low-density waveguides is an important current goal for laser-plasma accelerator research worldwide. This interest is motivated by the fact that the energy gain per stage varies[28] inversely with the electron density n_{e}, and the dephasing length (the distance over which the accelerating electron

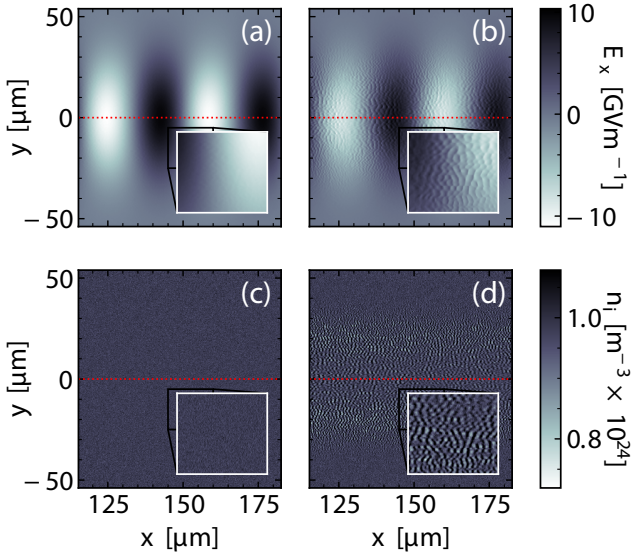

Figure 6: (a-b) Longitudinal electric field strength $E_x(x, y)$ as a function of longitudinal (x) and transverse (y) position, (a) 0.32 ps and (b) 2.56 ps after wake excitation, showing the development of high-frequency modulations of the field envelope, magnified in the inset. (c-d) Corresponding ion density $n_i(x, y)$, showing the development of high-frequency modulations. The red line indicates the axis of initial laser propagation.

bunch outruns the laser wakefield) varies as $L_{\rm d} \propto 1/n_{\rm e}^{3/2}$. Hence, compared to a 1 GeV accelerator, a 10 GeV stage requires operation at a plasma density an order of magnitude lower, and acceleration over a distance 30 times longer. For example, the nominal design point for the BELLA 10 GeV stage is[29] $n_{\rm e} = 0.96 \times 10^{17}\,{\rm cm}^{-3}$, $L = 600\,{\rm mm}$.

The length of a multi-GeV accelerator stage is much longer than the Rayleigh range (a few millimetres) and hence the drive laser pulse must be guided by some means. Although relativistic self-guiding has been used to reach GeV-scale energies, the resulting highly-nonlinear wakefield (a "plasma bubble") leads to self-injection of background electrons; this is difficult to control and often results in large energy spread and high shot-to-shot jitter of the bunch parameters.

It is therefore important to develop techniques for guiding intense laser pulses over 100s of millimetres of low density ($< 10^{18}\,{\rm cm}^{-3}$) plasma which are suitable for driving laser-plasma accelerators in the linear and quasilinear regime, including the MP-LWFAs discussed above. To take full advantage of the potential for MP-LWFAs to operate at high repetition rates, the waveguide must also be capable of high-repetition rate operation over extended periods. These are formidable challenges.

In this programme we have investigated a new technique developed by the PI, based on earlier work by Prof. Howard Milchberg at University of Maryland (UMD). In that earlier work,[30] a long column of plasma was formed, then heated, by a laser pulse focused with an axicon lens (a conical lens). Rapid radial expansion of the plasma column drove a shock wave into the surrounding gas to form a plasma channel. In this case the plasma column was heated (and further ionized) by electron-ion collisions driven by picosecond duration laser pulses. For the heating to be sufficiently fast the initial plasma density needed to be high, which limited the axial density of the plasma channel to values above $1 \times 10^{18}\,{\rm cm}^{-3}$.

The PI proposed[9,31] that plasma channels with low on-axis density, as required by multi-GeV accelerator stages, could be generated by hydrodynamic expansion of plasma columns formed and heated by optical field ionization (OFI). This ionization mechanism generates electrons with energies in the range 10 eV to 100 eV, and the mean electron energy can be controlled by adjusting the ellipticity of the laser field. Very importantly, since OFI operates at the atomic level, the electron heating is independent of the initial density, which allows the formation of low density plasma channels.

A particularly important feature of hydrodynamic plasma channels is that they could be operated at high repetition rates indefinitely since the plasma channel is not contained in a physical structure, and so is immune to damage by the incident laser pulses.

Prior to this research programme we had generated few-mm-long hydrodynamic optical-field-ionized (HOFI) plasma channels by using a conventional lens to focus a circularly-polarized, 50 fs laser pulse into hydrogen gas.[9] We measured the on-axis electron density and matched spot size of the channels to be in the range $1.5 \times 10^{17}\,{\rm cm}^{-3} \lesssim n_{\rm e}(0) \lesssim 1 \times 10^{18}\,{\rm cm}^{-3}$ and $61\,\mu{\rm m} W_{\rm M} \gtrsim 33\,\mu{\rm m}$ respectively.

In this section we outline the major advances and findings of our work to develop novel low-density plasma channels. Further details can be found in our associated journal publications.

4.2.1 Generation of HOFI channels with an axicon lens

We generated HOFI plasma channels with an axicon lens for the first time in experiments undertaken with the Astra-Gemini TA2 laser at CLF in three periods between 5th February 2018 and 5th July 2018 (CLF

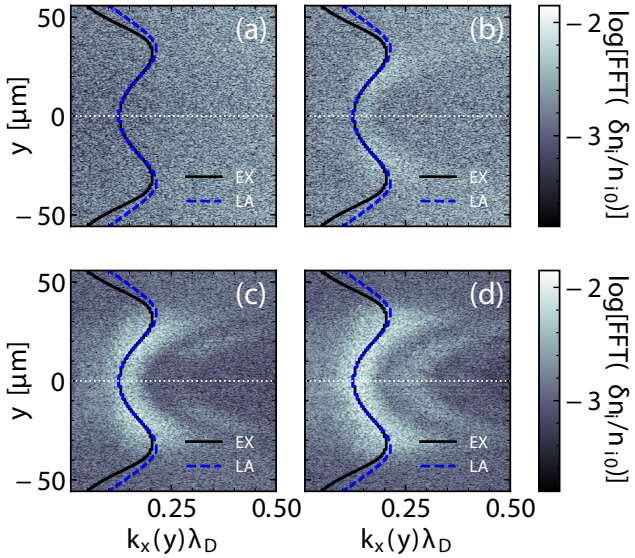

Figure 7: Longitudinal wave number spectrum $\log_{10}[{\rm FFT}_x(\delta n_i(x,y)/n_{i0})]$ of the perturbed ion density, as a function of transverse position y, at (a) $t = 0.64$ ps after wake excitation, (b) $t = 1.60$ ps, (c) $t = 2.56$ ps and (d) $t = 3.52$ ps. The instability initially grows fastest off-axis (b). The predicted transverse wave number dependence of the fastest growing mode is calculated by solving the dispersion relation derived by Sanmartin [27] (EX, black, solid line) and and an approximation to this, which is valid for a large driving field amplitude (LA, blue, dashed).

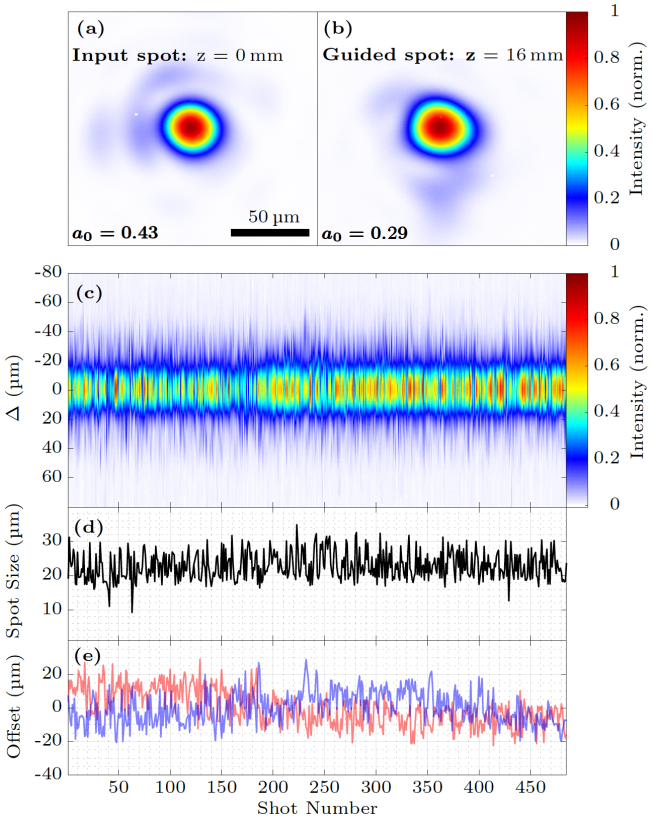

Figure 8: Laser guiding in HOFI plasma channels, showing transverse fluence profiles of the guided laser pulse at: (a) the entrance, and (b) the exit of a 16 mm long HOFI channel, at $\tau = 1.5$ ns. (c) shows, for each shot, the average of the horizontal and vertical fluence profiles through the centre of mass; the coordinate Δ has its origin at the centre of mass. In (d) the D4σ spot size[32] of the transmitted beam (averaged along the principal axes of the spot) is shown for each of the 485 shots; (e) shows the vertical (blue) and horizontal (red) offsets of the spot centre. In (a), (b), and (c) the peak fluence has been normalized to the highest value in each plot.

experiment 17210008). These results, which were analyzed during the first year of the current programme, have been published by Shalloo et al. [10].

Figure 8 demonstrates guiding of pulses with a peak input axial intensity of $4 \times 10^{17}\,\mathrm{W\,cm^{-2}}$ in a 16 mm long HOFI channel produced for an initial cell pressure of $P = 60$ mbar after a delay $\tau = 1.5$ ns between the arrival of the channel-forming pulse and the guided pulse. It can be seen that the transmitted transverse fluence profile of the guided beam measured at the channel exit (b) closely resembles that of the input beam (a), although it is very slightly elliptical. The orientation and degree of ellipticity was found to vary slightly with each shot, which is consistent with a shot-to-shot variation of the mode coupling arising from jitter in the transverse profile and pointing of the guided beam. To account for the slight ellipticity in the beam profile, the $D4\sigma$ spot size of the transmitted beam was calculated from the average of the spot size along the principal axes of the transmitted beam. The on-axis density of the channel was found from interferometric measurements to be $(3.6 \pm 0.9) \times 10^{17}\,\mathrm{cm^{-3}}$. In order to demonstrate the shot-to-shot stability of the HOFI channels, and to illustrate the potential for high repetition rate operation, the transverse intensity profiles of the guided beam were recorded for 485 consecutive shots, as summarized in Figs 8(c) - (e). These data were recorded in $f_{\mathrm{rep}} = 5$ Hz bursts of approximately 12 shots every 40 seconds, with free flowing hydrogen gas during each burst. The repetition rate was that of the laser system, and the duration and cadence of the bursts were limited by the available vacuum pumps. The mean spot size of the transmitted beams was found to be $(22.8 \pm 4.6)\mu$m, where the uncertainty is the root-mean-square (RMS) value over 485 shots. The RMS variation in the position of the centre of the transmitted beam was 14.1 μm, which is approximately twice that of the input beam.

The results shown in Fig. 8 demonstrate clearly the ability of HOFI channels to provide repeatable, high quality guiding of an intense beam over more than 14 Rayleigh ranges.

Plasma channels were generated with axial densities as low as $n_{\mathrm{e}}(0) = 1.5 \times 10^{17}\,\mathrm{cm^{-3}}$, with matched spot sizes in the range 20 µm $\lesssim W_{\mathrm{M}} \lesssim$ 40 µm. It was shown that these channels parameters could be controlled by adjusting the initial cell pressure, and the delay τ between the channel-forming and guided pulses. Highly reproducible, high-quality guiding of laser pulses with a peak input intensity of $4 \times 10^{17}\,\mathrm{W\,cm^{-2}}$ was demonstrated at a pulse repetition rate of 5 Hz.

4.2.2 Guiding of high-intensity pulses in 100 mm-long channels

We extended this work to generate, and demonstrate guiding in, 100 mm long HOFI plasma channels in experiments on optical guiding in HOFI plasma channels performed with the Astra-Gemini TA3 laser between 17th June and 4th August 2019 (CLF experiment 18210006). This work is described in Picksley et al. [6].

Figure 9 shows the experimental layout employed. Figure 10 demonstrates guiding of high-intensity

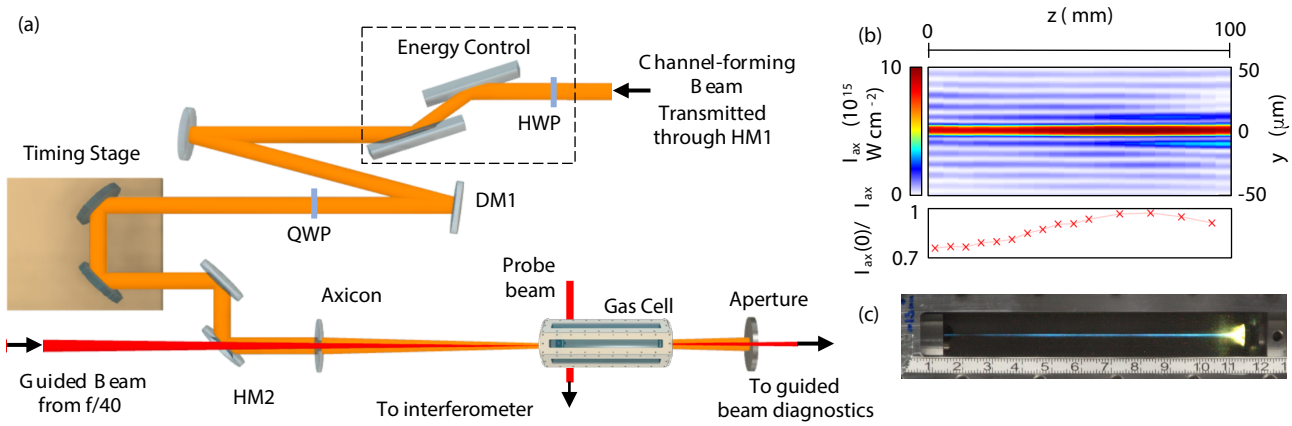

Figure 9: (a) Schematic diagram of the experiment layout used to study HOFI plasma channels with the Astra-Gemini TA3 laser. (b) Longitudinal variation of the transverse intensity profile of the axicon focus, measured in vacuo by a camera in the vacuum chamber. The red curve shows the axial intensity $I_{ax}(0)$ as a function of longitudinal position. (c) Time-integrated image of the visible plasma emission produced by the channel-forming beam focused into the gas cell at a fill pressure $P = 26$ mbar. The scale visible at the bottom of the image is in cm. Note that the apparent decrease in plasma brightness near a scale reading of 2.5 cm arises from blackening of the cell window in that region, not from non-uniformity of the plasma.

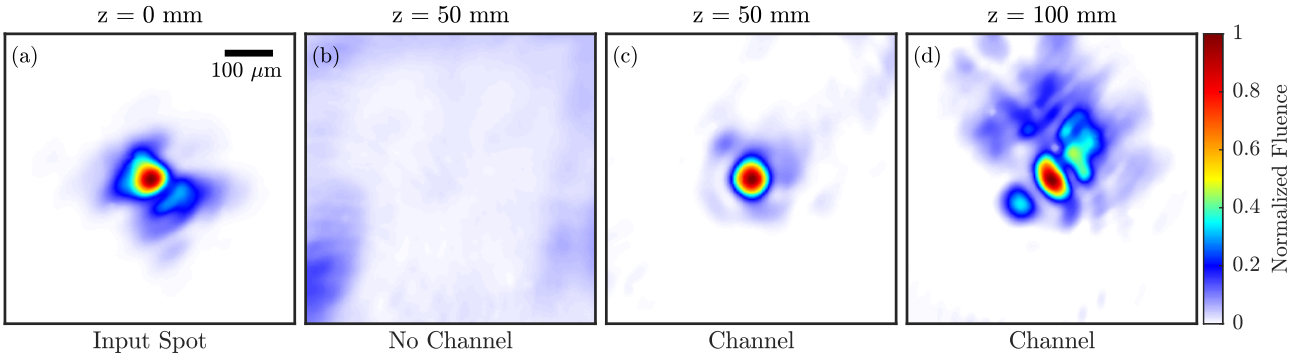

Figure 10: Measured transverse fluence profiles of the guided beam at: (a) focus, in vacuum; (b) $z = 50$ mm, in vacuum; (c) $z = 50$ mm, for $P = 68$ mbar and $\tau = 3.0$ ns; (d) $z = 100$ mm, for $P = 26$ mbar and $\tau = 2.7$ ns. The transverse scale is the same for all plots, as indicated by the scale bar shown in (a). For plots (a), (c), and (d) the fluence is normalized to the peak value in that plot; the fluence scale for (b) is the same as in (a). Compared to (a), the fluence scales of (c) and (d) were increased by factors of approximately 4 and 7 respectively.

laser pulses in HOFI channels up to 100 mm long. Figure 10(a) shows the transverse fluence profile of the input beam to be guided at its focus, recorded at full laser power. It can be seen that, despite the use of a deformable mirror, the input beam exhibited significant transverse structure. From this measured fluence profile the peak focused intensity is estimated to be 6.1×10^{17} W cm^{-2}.

Guiding was investigated in 50 mm and 100 mm long channels. For the shorter channels the guiding was approximately optimized by adjusting the initial cell pressure P and the delay τ between the channel-forming and guided laser pulses. For the input beam used in this work, the best guiding was found to occur at $P \approx 68$ mbar and $\tau \approx 3.0$ ns. For the 100 mm long channels the cell pressure was limited to $P \leq 26$ mbar; at this lower pressure the optimum delay was found to be $\tau \approx 2.7$ ns. Figure 10(b) shows the profile of the beam at $z = 50$ mm in the absence of a HOFI channel, showing clearly the effect of diffraction over a distance of more than $10 z_R$. Figure 10(c) shows the fluence profile in the same plane, but at a delay $\tau = 3.0$ ns after focusing the channel-forming beam into the cell filled to $P = 68$ mbar. The increase in the peak transmitted fluence is striking, and demonstrates clearly that the pulse was guided through the plasma channel generated by the channel-forming beam. For this pressure and timing, the on-axis density was measured to be $n_{e0} = (3.8 \pm 0.5) \times 10^{17}$ cm^{-3} and matched spot size $W_M = \left(30\,^{+5}_{-3}\right)$ μm. The energy transmission determined to be 27 %.

Fig. 10(d) shows the transverse fluence profile of the guided beam at the exit of a 100 mm long HOFI

channel formed at a similar delay ($\tau = 2.7$ ns), but at a lower cell pressure of 26 mbar. For this shot, the measured on-axis electron density was $n_{e0} = (1.0 \pm 0.3) \times 10^{17}\,\mathrm{cm}^{-3}$ and matched spot size $W_M = (34 \pm 7)\,\mu\mathrm{m}$. It is clear that guiding was also achieved in this case, the radius of the guided pulse was measured to be $w_{\mathrm{out}} = (48 \pm 14)\,\mu\mathrm{m}$, close to that of the focal spot. The measured energy transmission was 14 %. The low intensity light in the transverse wings can be attributed to the axicon light that reached the CCD, which is relatively more intense than in Fig. 10(c), or scattering from partially ionized gas at the exit of the waveguide.

Optical guiding was also observed in 50 mm long channels for cell pressures as low as 17 mbar. At this low pressure, it was not possible to measure the electron density profile interferometrically. However, the on-axis density was estimated to be $n_{e0} = 7 \times 10^{16}\,\mathrm{cm}^{-3}$ from simulations with the magneto-hydrodynamic (MHD) code HELIOS,[33] assuming cylindrical symmetry.

Figure 11 shows the energy transmission, $T(z)$, measured for several channel lengths and $P = 26$ mbar and $\tau = 2.7$ ns. It can be seen that the experimental data show an approximately exponential decrease in $T(z)$ with z; a fit of the expression $T(z) = T(0)\exp\left(-z/L_{\mathrm{att}}\right)$ to the data yields a coupling efficiency $T(0) = \left(45\,^{+14}_{-11}\right)\%$ and $L_{\mathrm{att}} = (102 \pm 38)$ mm.

Solving the paraxial Helmholtz equation[34,35] numerically allows the measured variation of the transmission with z to be compared with that expected for the measured transverse electron density profile of the channel. Figure 11 shows the results of these simulations for a channel with the transverse electron density profile measured for $P = 26$ mbar and $\tau = 2.7$ ns. For a Gaussian input beam, with spot size matched to that of the lowest-order mode of the channel, the coupling efficiency and attenuation length are found to be $T(0) \approx 100\%$ and $L_{\mathrm{att}} = (84 \pm 2)$ mm. This attenuation length is close to that observed in the experiment, but the coupling efficiency is much higher than is measured. This suggests that the lower measured values of $T(z)$ arise from the non-ideal transverse profile of the guided beam. To confirm this we used the same propagation code to simulate the propagation of a beam with an input transverse profile equal to that used in the experiment (see Fig. 10(a)), assuming a flat transverse spatial phase. As shown in Fig. 11, the calculated energy transmission for the real input beam agrees well with the measured data. We note that the non-exponential variation in $T(z)$ observed for $z \lesssim 30$ mm arises from the excitation of higher-order modes, which have higher propagation losses; as expected, for larger values of z the rate of decrease of $T(z)$ closely follows that of the lowest-order mode. The attenuation length and coupling efficiency for the experimentally-measured input beam was deduced by fitting an exponential decay to the calculated transmission in the region $z \geq 50$ mm, where the guided beam is dominated by the lowest order mode. The attenuation length is found to be $L_{\mathrm{att}} = (84 \pm 2)$ mm, which agrees with the measured value to within errors, and is equal to that calculated for a matched input beam. The calculated coupling efficiency for the experimentally-measured input beam is $T(0) = (48 \pm 4)\,\%$. This coupling efficiency agrees well with an expansion of the input spot shown in Fig. 10(a) as a superposition of Laguerre-Gauss modes, with a spot size equal to the matched spot size of the channel: this shows the fractional power contained in the lowest-order Laguerre-Gauss mode is $(49 \pm 8)\,\%$.

As we discuss below, it is likely that the guiding observed in this work will have been assisted by ionization of the neutral or partially ionized gas surrounding the plasma channel, since ionization of this type would have increased the channel depth. The guiding simulations do not include this effect, but they do show that the laser field immediately outside the channel can be high. For example, in the simulations of matched guiding shown in Fig. 11, the ratios of the peak laser intensity at $2r_{\mathrm{shock}}$ to that on axis is calculated to be 0.5%. Hence, for the guided intensities achieved in this work, the laser fields leaking beyond the shock front would be sufficient to ionize any neutral gas in this region.

In summary, in this work we demonstrated the generation of HOFI channels with lengths up to 100 mm. Optical guiding of laser pulses with a peak input intensity of $6 \times 10^{17}\,\mathrm{W\,cm}^{-2}$ was demonstrated over $21 z_{\mathrm{R}}$ in plasma channels as low as $n_{\mathrm{e}}(0) = (1.0 \pm 0.3)\,\mathrm{cm}^{-3}$. The measured energy transmission was dominated by the relatively poor coupling of the non-ideal input beam, and by the measured power attenuation length of $L_{\mathrm{attn}} \approx 100$ mm. Guiding was also observed at lower fill pressures, for which MHD simulations predict the on-axis plasma density to be as low as $n_{\mathrm{e}}(0) \approx 7 \times 10^{16}\,\mathrm{cm}^{-3}$.

Analysis showed that the coupling efficiency achieved in this work, $T(0) = (45^{+14}_{-11})\%$ was limited by unwanted structure in the transverse profile of the input beam.

To our knowledge these plasma channels are the longest, and have the lowest on-axis density, of any free-standing plasma channel demonstrated to guide laser pulses with intensities above $1 \times 10^{17}\,\mathrm{W\,cm}^{-2}$. They were generated with only 0.7 mJ of channel-forming laser energy per millimetre of channel.

4.2.3 Metre-scale conditioned HOFI (CHOFI) plasma channels

A major breakthrough in our work on the development of low density plasma channels was the realization that the hydrodynamic expansion of the initial plasma column created a "collar" of neutral gas that surrounded

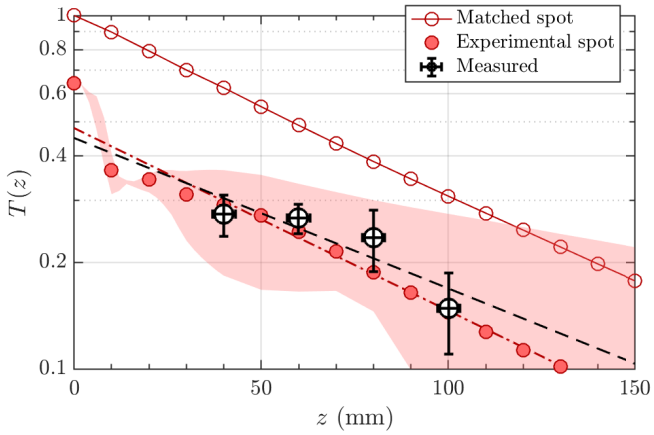

Figure 11: Comparison of the measured and simulated energy transmission for plasma channels formed at $P = 26\,\text{mbar}$ and $\tau = 2.7\,\text{ns}$. The measured data is shown as open black circles, with error bars with a total length equal to one standard deviation. The dashed black line shows a fit of the function $T_{\text{theory}}(z) = T(0)\exp(-z/L_{\text{att}})$ to the experimental data. The open red circles show the calculated transmission for the lowest-order mode of the channel. The solid red circles show the calculated energy transmission for an input beam with a transverse intensity profile equal to the experimentally-measured profile (see Fig. 10(a)); the red shading shows the uncertainty in $T(z)$ arising from the the uncertainties in the electron density profile. The red dash-dot line shows a fit of the function $T_{\text{theory}}(z)$ to the calculated transmission for the realistic input spot in the region $z > 50\,\text{mm}$.

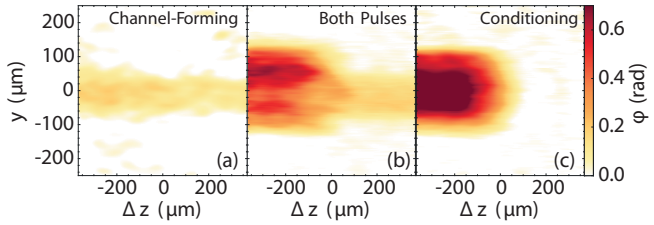

Figure 12: Transverse interferometry of HOFI and CHOFI channels. (a-c) Phase shifts measured by the transverse probe beam at $z \approx 3.5\,\text{mm}$ for: (a) the channel-forming pulse alone, (b) the channel-forming pulse and the conditioning pulse at a delay $\tau = 1.5\,\text{ns}$; and (c) the conditioning pulse alone

the HOFI channel. This was observed in the 2018 Astra-Gemini TA2 experiments,[10] and first described in.[11] Our work in this area benefitted considerably from later work by Feder, Miao, Shrock, Goffin and Milchberg [36], in which two-colour interferometry was used to observe and characterize the collar of neutral gas.

Figure 12 shows the results of transverse interferometry of the plasma channel, and captures the moment when the guided pulse arrives, at $\tau = 1.5\,\text{ns}$ after the channel-forming pulse. In Fig. 12(b) the guided pulse has reached the point $\Delta z = 0$, so that the region of positive z contains plasma generated by the channel-forming pulse alone, whereas the region $\Delta z < 0$ contains plasma formed by both pulses. It is clear that the guided pulse increases the radial extent of the plasma by a factor of approximately 5 from that produced by the channel-forming pulse alone. Further, the radial extent of the plasma generated by both pulses is essentially the same as that of the plasma produced by the guided pulse alone, as shown in Fig. 12(c). It is clear from Fig. 12 that the transverse wings of the guided pulse ionize neutral gas surrounding the HOFI plasma channel. As we see below, this additional ionization deepens the plasma channel considerably, greatly reducing the propagation losses of the channel. In this context we therefore refer to the guided pulse as a "conditioning" pulse, and the channels that are formed as conditioned HOFI (CHOFI) plasma channels.

Figure 13 shows the formation and temporal evolution of the transverse electron density profile of the CHOFI channels, obtained by Abel inversion of retrieved phase shifts like that shown in Fig. 12. Figure 13(a) shows the electron density profile before and immediately after the arrival of the conditioning pulse at $\tau = 1.5\,\text{ns}$. It can be seen that the conditioning pulse has little effect on the electron density for radii within the radius of the shock front, $r_{\text{shock}} \approx 25\,\mu\text{m}$, created by the channel-forming pulse. However, at larger radii the electron density is increased substantially to form a deep, thick-walled CHOFI plasma channel: the depth of the channel was increased by a factor of 10 to $\Delta n_{\text{e}} = (1.3 \pm 0.1) \times 10^{18}\,\text{cm}^{-3}$; whereas, within the experimental uncertainty, the axial density remained at $n_{\text{e0}} = (2.4 \pm 1.0) \times 10^{17}\,\text{cm}^{-3}$. The radial extent of the plasma was increased by the conditioning pulse from $r_{\text{shock}} \approx 25\,\mu\text{m}$ to $r_{\text{max}} \approx 120\,\mu\text{m}$.

As shown in Fig. 13, the electron density in the region $r > r_{\text{shock}}$ is comparable to that expected for full ionization of the initial ambient gas, consistent with field ionization of the neutral gas by the transverse wings of the conditioning pulse. It is noticeable that in the region close to $r \approx 50\,\mu\text{m}$ the electron density is greater than that which would be generated by ionization of the neutral gas at its ambient density; this

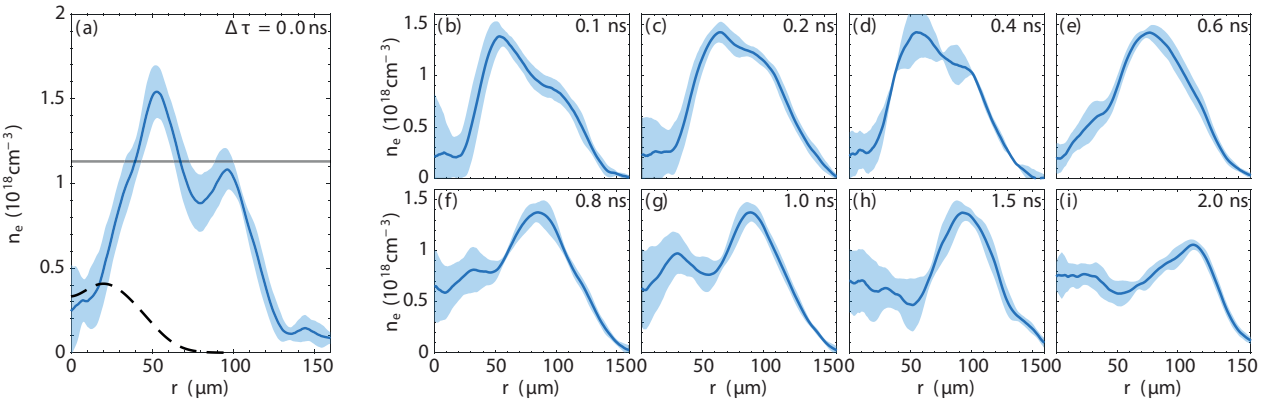

1

Figure 13: Formation and temporal evolution of the transverse electron density profiles $n_e(r)$ in the CHOFI waveguide. (a) Measured electron density profile immediately before (dashed) and after (solid) the arrival of the conditioning pulse at $\tau = 1.5$ ns ($\Delta\tau = 0$ ns). The horizontal, grey line shows the density corresponding to full ionization of the ambient gas. (b)-(i) Electron density profiles measured at different additional delays $\Delta\tau$ (indicated) after the arrival of the channel-forming pulse, for a conditioning pulse arriving at $\tau = 1.5$ ns. All plots show the mean of approximately 20 shots recorded at a repetition-rate of 5 Hz, with the probe pulse crossing at $z \approx 3.5$ mm with respect to the front pinhole. The data is averaged longitudinally over approximately 0.75 mm. The shaded region is one standard deviation wide.

is consistent with a build up of neutral gas at the shock front as it pushes the gas outwards.

The evolution of the plasma at various delays $\Delta\tau$ after the arrival of the conditioning pulse at $\tau = 1.5$ ns is shown in Fig. 13(a)-(i). For $\Delta\tau = 0.2$ ns, the measured axial density remained approximately the same, and the channel wall thickened slightly. At longer delays $\Delta\tau$, electrons in the high density ring spread radially outwards and inwards, which causes the position of the peak density to increase to $r = 100$ μm by $\Delta\tau \approx 1$ ns and the axial density to increase. Even at $\Delta\tau \approx 2$ ns, where the channel structure has begun to decay, the measured channel depth was greater than before the arrival of the conditioning pulse.

Hydrodynamic simulations were undertaken to understand in detail the distribution of plasma and neutral gas prior to the arrival of the conditioning pulse. These were performed in two dimensions, using the Eulerian code FLASH.[37] Figure 14 summarizes the results of these simulations, and shows the temporal evolution of the electron and neutral gas transverse density profiles. The formation of a neutral collar of gas as the plasma column expands radially is evident. It is this collar which can be ionized by a subsequent conditioning pulse to form a deep CHOFI channel.

Figure 15 summarizes the results of PIC simulations of the formation of a CHOFI channel. Close to the channel entrance, the far leading edge of the pulse ionizes the neutral gas surrounding the HOFI channel,

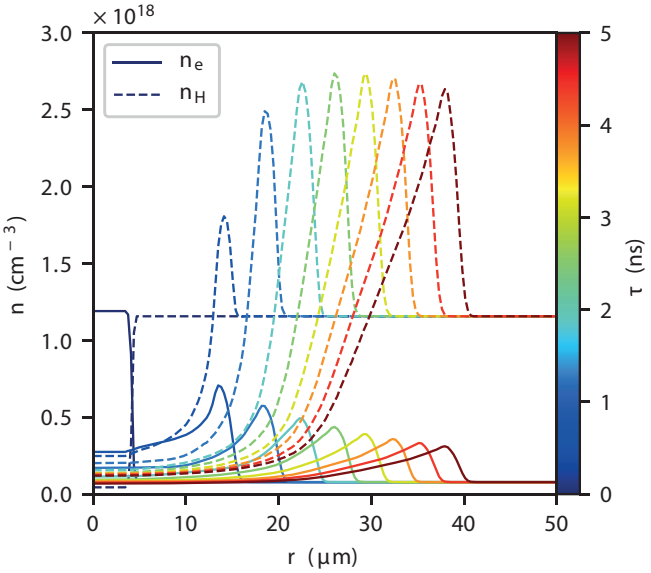

Figure 14: Hydrodynamic simulation of a HOFI channel, showing the temporal evolution of the electron (n_e, straight) and neutral hydrogen (n_H, dashed) transverse density profiles at various delays τ given by the color scale.

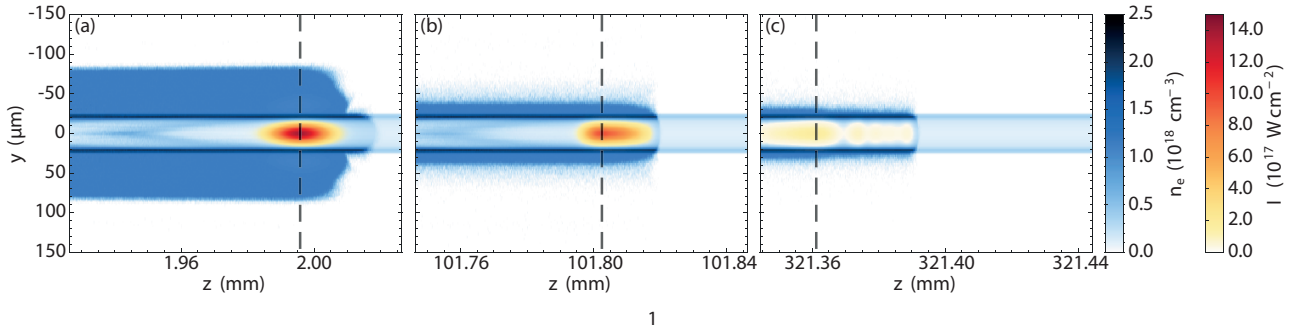

Figure 15: Transverse profiles of the electron density and the laser intensity when the peak of the conditioning pulse, indicated by the dashed line, has reached (a) $z = 2\,\mathrm{mm}$, (b) $z = 101\,\mathrm{mm}$, and (c) $z = 321\,\mathrm{mm}$. The input intensity of the conditioning pulse was $I_{\mathrm{peak}} = 6.0 \times 10^{17}\,\mathrm{W\,cm^{-2}}$.

creating a deep CHOFI channel in which the main body of the pulse is guided. Since the transverse intensity profile of the conditioning pulse is not perfectly matched to that of the lowest order mode of either the HOFI or CHOFI waveguides, the spot-size of the conditioning pulse oscillates by $\pm 10\,\%$ during the first few centimetres of propagation. However, this variation primarily affects the wall thickness of the CHOFI channel, not its depth or matched spot size. Further, the higher-order modes excited by the conditioning pulse are attenuated with propagation, and the conditioning pulse adopts a stable configuration. This situation is shown in Fig. 15(b-c), which shows that the radial extent of the additional ionization is reduced with propagation distance z. However, the high walls of the CHOFI channel remain, and are sufficiently thick, to ensure low-loss propagation of the bulk of the conditioning pulse. The conditioning pulse continues to propagate with low loss, and to generate a low-loss channel, until it can no longer ionize the neutral gas close to the shock front.

These results show that the leading edge of a conditioning pulse can ionize the neutral gas surrounding HOFI plasma channels, to form a conditioned HOFI channel with very low losses. This mechanism is likely to have played a role in the work described in §4.2.2.

The simulations shown in Fig. 15 demonstrate the formation of channels up to 325 mm long.

The conditioning pulse is self-guided, which has three important consequences. First, as discussed below, the energy of the conditioning pulse is used efficiently, which reduces the total laser energy required to create the CHOFI channel. Second, the generated CHOFI channel is robust to variations of the parameters or pointing of the conditioning pulse. Third, a wide range of channel parameters and shapes are accessible with a simple experimental setup. We note that the conditioning pulse does not require transverse shaping and should have the same spot size and central wavelength as the main pulse to be guided; as such, it could be generated very simply by introducing a small prepulse to the main pulse.

Estimates[7] of the total laser energy required to generate a CHOFI channel show that approximately 5 mJ is required to generate each centimetre of the initial HOFI channel, and a further $7\,\mathrm{mJ\,cm^{-1}}$ is required for conditioning. Hence a 1 m long CHOFI channel would require a total laser energy of 1.2 J, which is modest compared to the laser energy required to drive a metre-scale laser-plasma accelerator.

In summary, in this work we demonstrated that low density plasma channels with lengths on the metre scale could be generated by conditioning HOFI channels. Channels with axial electron densities of $n_{\mathrm{e}}(0) \approx 1 \times 10^{17}\,\mathrm{cm^{-3}}$ and matched spot size $W_{\mathrm{M}} \approx 25\,\mu\mathrm{m}$ were generated experimentally. These channels had power attenuation lengths as long as $L_{\mathrm{attn}} \approx 20\,\mathrm{m}$. These channels would appear to be ideally suited to multi-GeV plasma accelerator stages.

4.2.4 kHz HOFI channels

One of the crucial potential advantages of HOFI and CHOFI channels is that they could operate at high repetition rates for extended periods. We tested these claims in experiments performed in the Oxford Plasma Accelerator Laboratory (OPAL). This work has been published.[38]

The experiments were carried using the kHz repetition-rate front-end of a 12 TW Ti:sapphire laser system. A schematic of the experimental setup is shown in Fig. 16. The front-end of the OPAL laser system delivered an energy of $(1.05 \pm 0.02)\,\mathrm{mJ}$ per pulse, compressed to a pulse duration of $(39 \pm 2)\,\mathrm{fs}$ full-width-at-half-maximum (FWHM). In order to investigate the formation of channels at different repetition rates, a pulse picker — comprising a pair of polarising beam splitters (P-BS) and a Pockels cell — was located before the CPA compressor. This could select two or more pulses spaced by an integer multiple of 1 ms.

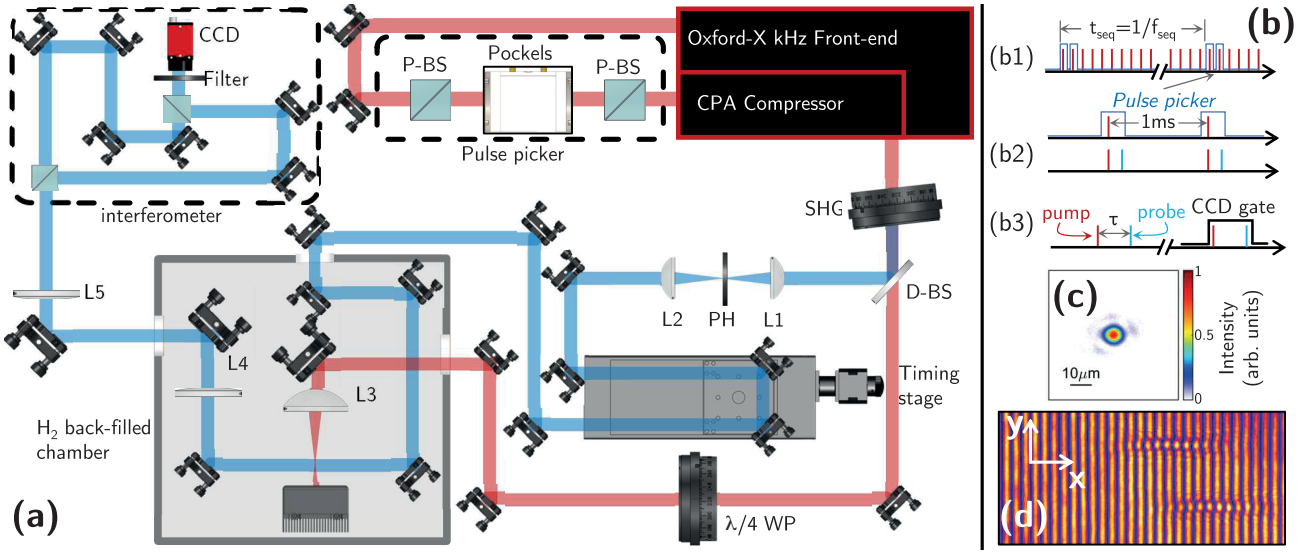

Figure 16: **(a)** Schematic diagram of the experimental setup used to generate HOFI plasma channels at kHz repetition rates. See the main text for a detailed description. **(b)** Schematic diagram of the generation of probe and pump pulses, showing: (b1) the train of 800 nm pulses from the laser front-end, and the selection of pairs of 800 nm pulses, the pairs being separated by $t_{\rm seq} = 1/f_{\rm seq}$; (b2) the conversion of each pair of pulses into a pump-probe pair; and (b3) gating of the CCD to record the interferogram generated by the second pump-probe pair. **(c)** Measured focal spot of the channel-forming beam. **(d)** Raw interferogram measured 50 ps after the passing of the channel-forming beam, using a 350 mbar backfill pressure of H_2.

The experiments employed a pump-probe arrangement in which the pump (or 'channel-forming') pulse generated the HOFI plasma channel, and the probe pulse was used to characterise its evolution. In order to generate the pump and probe beams, pulses selected by the pulse picker, and compressed by the grating compressor, were propagated through a Second Harmonic Generation (SHG) crystal. For each pulse incident on the SHG crystal, a small fraction was converted to a probe pulse with a wavelength of 400 nm. The remaining 800 nm pulse, of energy of ~1 mJ, constituted the co-propagating channel-forming pulse.

The 800 nm channel-forming beam was focussed into a vacuum chamber by an $f' = 30$ mm convex lens (L3) to a focus of 5 µm FWHM. Plasma channels were formed by filling the chamber with H_2 gas at a pressure in the range $P_{\rm b}$ =50 mbar to 500 mbar.

The 400 nm-probe beam was used for transverse interferometry of the HOFI channels. A timing stage allowed the delay τ between the arrival of the channel-forming pulse and the arrival of the probe pulse (at their intersection) to be varied.

The maximum repetition rate at which data could be recorded was limited by the readout time of the camera, which was several milliseconds when the full field of view of the camera was recorded (500 µm × 375 µm). In order to prevent the camera from capturing interferograms generated by multiple probe pulses, the pulse picker was used to produce either a single 800 nm pulse, or a pair of such pulses separated by 1 ms. For the case of two channel-forming pulses, the CMOS camera could be triggered to capture the interferogram generated by the second probe pulse only. By examining the channels formed by a single channel-forming pulse, and that produced by the second of a pair of such pulses, it was possible to investigate whether the plasma formed by the first pulse influenced the channel formed 1 ms later. These pulse sequences were generated at a repetition rate of $f_{\rm seq} = 10$ Hz, which was the rate at which data was collected.

Figure 17 shows the temporal evolution of the transverse electron density profile $n_{\rm e}(r)$ of HOFI plasma channels generated by single channel-forming pulses, and by the second of a pair of such pulses separated by 1 ms. The evolution of the channels formed by a single pulse is consistent found in our earlier experiments.[9,10] As seen in Fig. 17, the channel formed by the *second* of a pair of channel-forming pulses separated by 1 ms is almost identical to that formed by a single pulse. It can therefore be concluded that, even with a static gas fill, the plasma cools and recombines to form an approximately uniform gas within 1 ms, consistent with the absence of plasma in the interferogram measured immediately prior to the arrival of the second pulse.

In order to investigate whether HOFI channels could be generated at kHz repetition rates for an extended period, interferograms were recorded with a reduced field of view of 135 µm × 100 µm, which allowed data to be recorded for pairs of channel-forming pulses separated by 1 ms at a pulse sequence repetition rate of $f_{\rm seq} = 200$ Hz, and hence a mean pulse repetition rate of $\langle f_{\rm rep} \rangle = 0.4$ kHz.

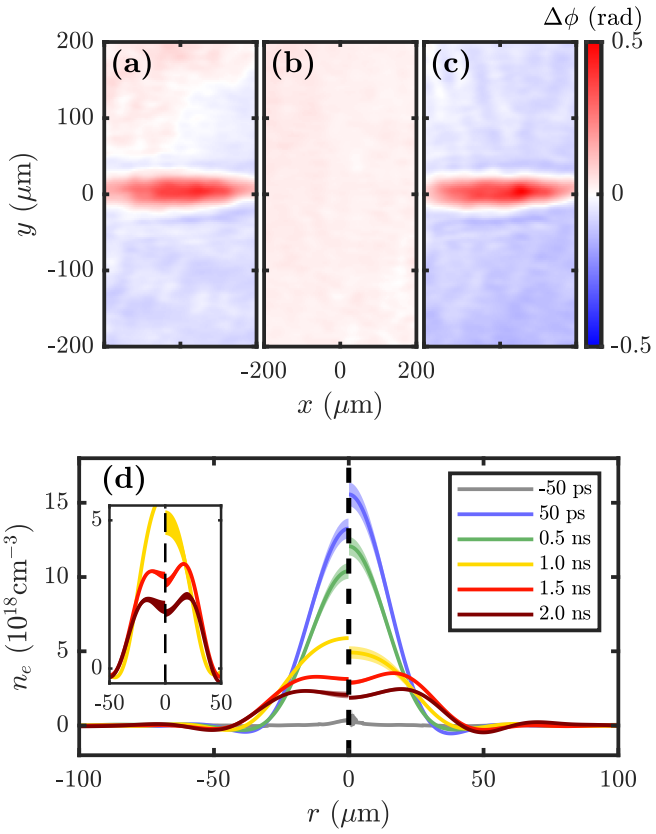

Figure 17: **(a,b,c)** Phase maps retrieved from the interferometric measurements. (a,c) show the plasma generated by (a) a single channel-forming pulse, and (c) the second of a pair of channel-forming pulses separated by 1 ms, measured at $\tau = 0.5$ ns after the passing of the channel-forming beam. (b) Measured phase shift 50 ps prior to the arrival of the second channel-forming pulse. **(d)** Temporal evolution of the transverse electron density profile $n_e(r)$ produced by: (left) a single channel-forming pulse; and (right) the second of a pair of channel-forming pulses separated by 1 ms. For each plot the line and shading show, respectively, the average and standard deviation of the density measured over 50 shots. For these data $P_b = (350 \pm 3)$ mbar. The inset in (d) depicts a zoom-in of the electron density profiles for $\tau \geq 1$ ns, clearly showing the plasma channel formed at those times.

Figure 18 shows the transverse electron density profiles of the HOFI channels, formed at a delay $\tau = 1.5$ ns after the second of the pair of channel-forming pulses, recorded at $f_{seq} = 200$ Hz over a period of 6.5 hours. It can be seen that HOFI channels were created throughout this period, with no significant long-term evolution of their properties. These data demonstrate that slow heating of the gas will not have a deleterious effect on the channels for mean repetition rates at least up to 0.4 kHz.

Further analysis of these data was undertaken to determine the shot-to-shot jitter and long-term evolution of the key channel properties during the 6.5 hour run. This analysis showed that the measured jitter in these parameters was dominated by the effects of noise in the measurement. It is expected that relatively small long-term drift in the channel parameters that was observed could largely be eliminated by adding feedback systems to the gas and laser control systems.

In summary, we demonstrated that two HOFI channels generated within 1 ms of each other were essentially the same. We also showed that HOFI channels can be generated at a repetition rate of 0.4 kHz for a period of 6.5 hours with no degradation of the channel parameters. These findings are also expected to hold for CHOFI channels.

These results were obtained for a static gas cell. If necessary, it might be possible to operate at higher pulse repetition rates by flowing the gas transversely in order to replace the gas between shots. A simple analysis[38] suggests that repetition rates as high as 1 MHz could be achieved with this geometry.

4.2.5 Controlled electron injection and acceleration in CHOFI channels

The experiment was performed with the Astra-Gemini TA3 laser at CLF (experiment no. 20110003) over a total of six weeks between October 2021 and January 2022. The primary aim of this experiment was to demonstrate controlled electron injection into low density ($n_e \approx 1 \times 10^{17}$ cm^{-3}) plasma channels for the first time.

In these experiments a 110 mm long HOFI channel was generated using the set-up described in §4.1.2. For these experiments the gas cell was filled with a 98:2% hydrogen-nitrogen mixture. The on-axis plasma density was $(1.3 \pm 0.1) \times 10^{17}$ cm^{-3}.

A drive pulse, with a duration of approximately 40 fs, and a total energy of 6 J was focused at $f/40$ to the entrance of the HOFI channel. Electrons were injected into the wakefield via a novel technique — which we call "truncated-channel injection"(TCI) — by exploiting the density down-ramp that is naturally formed between the ambient gas and the start of the plasma channel.

Figure 19(a) shows the measured injection success as a function of the longitudinal position of the leading edge of the channel with respect to the longitudinal position of the focus of the drive pulse (Δz). Electron injection was consistently observed simultaneously with guiding when the drive pulse focus interacted with

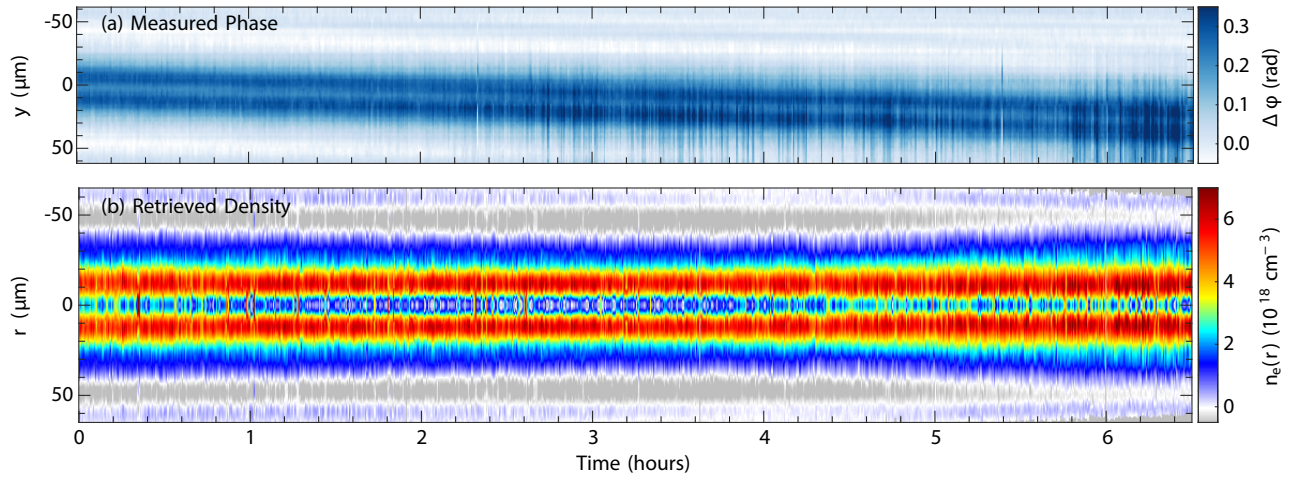

Figure 18: Demonstration of the long-term stability of HOFI channels. **(a)** The measured phase map; the apparent slow drift in the transverse position of the plasma is an artifact caused by a slow drift in the position of the probe beam. **(b)** The transverse electron density profiles of the HOFI channels formed at a delay $\tau = 1.5$ ns after the second of the pair of channel-forming pulses separated by 1 ms are shown for data recorded at $f_{\rm seq} = 200$ Hz over a period of 6.5 hours. For these data the initial gas pressure was $P_{\rm b} = 350$ mbar.

the leading edge of the channel ($\Delta z \approx 0$). As shown in Fig. 19(b), when the drive pulse was well-aligned with the channel ($\delta r \leq 10\,\mu$m), mean electron energies in excess of 1 GeV were measured with energy spreads on the percent-level, indicating high-quality, localised injection triggered by TCI. As the axicon was was translated upstream ($\Delta z < -5$ mm) — i.e. the channel started well before the laser focus — electron beams were only observed if the drive pulse was misaligned with the channel, and these beams were of low quality. This behaviour is likely to have been caused by the mis-directed drive beam interacting with the high density walls of the plasma channel, thereby triggering injection.

The characteristics of electron bunches generated via TCI were compared to those from ionisation injection, a well-established electron injection technique that relies on the peak fields of the laser pulse locally ionising inner-shell electrons from a dopant gas species such that they are born within the wakefield, trapped and accelerated. Ionization injection of the nitrogen dopant was found to be triggered by increasing the on-axis plasma density to $n_{\rm e0} = (2.2 \pm 0.1) \times 10^{17}$ cm^{-3}, while the axicon was translated far upstream ($\Delta z = -11.2$ mm) to avoid TCI. As shown in Fig. 19(b), electron bunches injected via TCI had consistently higher mean energies than for ionisation injection and, crucially, when well-aligned with the guiding channel ($\delta r \leq 10\,\mu$m) had much reduced energy spread and improved energy stability. This indicates control of the injection process with TCI, as electrons are only injected within the density transition at the channel entrance rather than over an extended region of the channel, as is the case for ionisation injection.

In summary, we successfully demonstrated injection and acceleration of high-quality electron bunches in low density plasma channels. This was achieved using a novel and simple injection technique: truncated-channel injection. Electron bunches, with total charge in the pC range, were accelerated to energies in excess of 1 GeV with percent-level energy spreads. Our on-going simulations of the TCI process have indicated that the electron energies achieved in this experiment were limited only by the length of the target, and suggest that high-quality electron bunches with energies in excess of 4.5 GeV could be generated with identical laser parameters in a 400 mm long plasma channel. A paper describing this work is being prepared for publication.

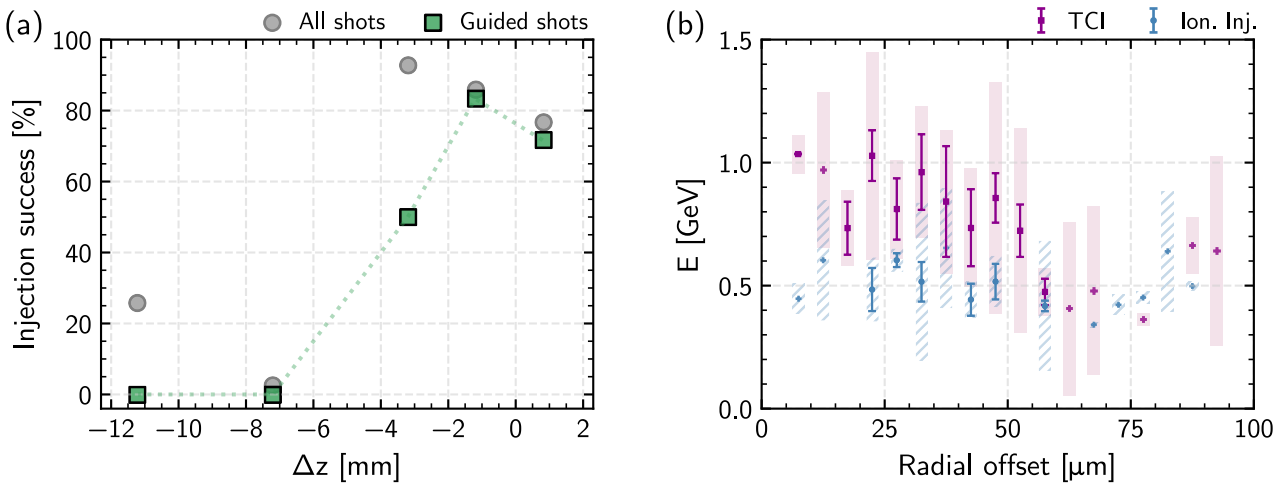

Figure 19: Preliminary analysis of experiments to demonstrate controlled electron injection and acceleration in low density plasma channels. (a) Measured injection success as a function of the relative longitudinal positions of the leading edge of the channel and the drive pulse focus (Δz). When considering events with successful guiding (green), electron injection is only observed for $\Delta z \geq -3.2\,\mathrm{mm}$, when there is significant overlap between the front edge of the channel and the drive pulse focal position. (b) Comparison between accelerated electron bunch properties as a function of radial offset (δr) of the drive pulse with respect to the channel entrance for truncated channel injection (purple, squares) and ionisation injection (blue, circles). Data points and error bars represent the average mean energy and associated standard error within 5 μm-wide bins. The average RMS energy spread of electron bunches within each bin is represented by the shaded regions. Bins with only a single event are represented by '+' markers.

5 References

[1] C. Arran. "Techniques for High Repetition Rate Laser Wakefield Acceleration". PhD thesis. University of Oxford, 2018.

[2] J. Jonnerby. "Multi-pulse laser wakefield acceleration". PhD thesis. University of Oxford, 2021.

[3] A. von Boetticher, R. Walczak and S. M. Hooker. "Modulational instability in large-amplitude linear laser wakefields". In: *Submitted* (2022).

[4] A. von Boetticher. "Topics in laboratory plasma instability and turbulence". PhD thesis. University of Oxford, 2021.

[5] O. Jakobsson, S. M. Hooker and R. Walczak. "Gev-Scale Accelerators Driven by Plasma-Modulated Pulses from Kilohertz Lasers". In: *Physical Review Letters* 127.18 (2021), p. 184801. ISSN: 0031-9007. DOI: 10.1103/physrevlett.127.184801. eprint: 2110.00417.

[6] A. Picksley et al. "Guiding of high-intensity laser pulses in 100-mm-long hydrodynamic optical-field-ionized plasma channels". In: *Physical Review Accelerators and Beams* 23.8 (Aug. 2020), p. 081303. DOI: 10.1103/physrevaccelbeams.23.081303.

[7] A. Picksley et al. "Meter-scale conditioned hydrodynamic optical-field-ionized plasma channels". In: *Physical Review E* 102.5 (Oct. 2020), p. 053201. DOI: 10.1103/physreve.102.053201.

[8] C. Arran, N. H. Matlis, R. walczak and S. M. Hooker. "Reconstructing nonlinear plasma wakefields using a generalized temporally encoded spectral shifting analysis". In: *Phys. Rev. Accel. Beams* 21.10 (Oct. 2018), p. 103501. DOI: 10.1103/PhysRevAccelBeams.21.103501.

[9] R. J. Shalloo et al. "Hydrodynamic optical-field-ionized plasma channels". In: *Phys Rev E* 97 (May 2018), p. 053203. DOI: 10.1103/PhysRevE.97.053203.

[10] R. J. Shalloo et al. "Low-density hydrodynamic optical-field-ionized plasma channels generated with an axicon lens". In: *Phys. Rev. Accel. Beams* 22.4 (Apr. 2019), p. 041302. DOI: 10.1103/PhysRevAccelBeams.22.041302.

[11] R. J. Shalloo. "Hydrodynamic optical-field-ionized plasma waveguides for laser plasma accelerators". PhD thesis. University of Oxford, 2018.

[12] T. Nakada. *European Strategy for Particle Physics - Accelerator R&D Roadmap*. Tech. rep. Geneva: CERN, 2022, pp. 1–270.

[13] C. Geddes, M. Hogan, P. Musumeci and R. Assmann. "Report of Snowmass 21 Accelerator Frontier Topical Group 6 on Advanced Accelerators". In: *arXiv* (2022). eprint: 2208.13279.

[14] S. M. Hooker et al. "Multi-pulse laser wakefield acceleration: a new route to efficient, high-repetition-rate plasma accelerators and high flux radiation sources". In: *Journal Of Physics B-Atomic Molecular And Optical Physics* 47.23 (Nov. 2014), pp. 1–14. DOI: 10.1088/0953-4075/47/23/234003.

[15] C. Herkommer et al. "Ultrafast thin-disk multipass amplifier with 720 mJ operating at kilohertz repetition rate for applications in atmospheric research". In: *Optic Express* 28.20/28 (2020), p. 30164. DOI: 10.1364/OE.404185.

[16] T. Produit et al. "The Laser Lightning Rod project". In: *The European Physical Journal Applied Physics* 92 (2020), p. 30501. ISSN: 1286-0042. DOI: 10.1051/epjap/2020200243.

[17] Y. Wang et al. "1.1 J Yb:YAG picosecond laser at 1 kHz repetition rate". In: *Optics Letters* 45.24/15 (2020), p. 6615. DOI: 10.1364/OL.413129.

[18] J. J. Rocca et al. "High average power femtosecond laser driver for plasma accelerators by compression of spectrally broadened high energy Yb:YAG laser pulses". In: *Snowmass 2021 AF7/AF6: Advanced Accelerator Concepts*. 2021.

[19] G. Fan et al. "70 mJ nonlinear compression and scaling route for an Yb amplifier using large-core hollow fibers". English. In: *Optics Letters* 46.4 (2021), pp. 896–4. DOI: 10.1364/ol.412296.

[20] M. Kaumanns, D. Kormin, T. Nubbemeyer, V. Pervak and S. Karsch. " Spectral broadening of 112 mJ, 1.3 ps pulses at 5 kHz in a LG_{10} multipass cell with compressibility to 37 fs ". In: *Optics Letters* 46.5 (2021), p. 929. ISSN: 0146-9592. DOI: 10.1364/ol.416734.

[21] E. Esarey, A. Ting and P. Sprangle. "Frequency shifts induced in laser pulses by plasma waves". In: *Physical Review A* 42.6 (1990), p. 3526.

[22] T. D. Arber et al. "Contemporary particle-in-cell approach to laser-plasma modelling". In: *Plasma Physics and Controlled Fusion* (Sept. 2015), pp. 1–26. DOI: 10.1088/0741-3335/57/11/113001.

[23] J. Cowley et al. "Excitation and Control of Plasma Wakefields by Multiple Laser Pulses". English. In: *Phys Rev Lett* 119.4 (July 2017), pp. 044802–6. DOI: 10.1103/PhysRevLett.119.044802.

[24] J. Derouillat et al. "Smilei: A collaborative, open-source, multi-purpose particle-in-cell code for plasma simulation". In: *Computer Physics Communications* 222 (2018), pp. 351–373. ISSN: 0010-4655. DOI: https://doi.org/10.1016/j.cpc.2017.09.024.

[25] A. A. Vedenov and L. I. Rudakov. "Wave interaction in continuous media". In: *Dokl. Akad. Nauk SSSR* 159.4 (1964), p. 767.

[26] V. E. Zakharov. "Collapse of Langmuir waves". In: *Zh. Eksp. Teor. Fiz* 35 (5 Nov. 1972), pp. 1867–1870.

[27] J. R. Sanmartin. "Electrostatic plasma instabilities excited by a high-frequency electric field". In: *The Physics of Fluids* 13.4 (June 1970), p. 1533.

[28] E. Esarey, C. B. Schroeder and W. P. Leemans. "Physics of laser-driven plasma-based electron accelerators". English. In: *Rev. Mod. Phys.* 81.3 (Aug. 2009), pp. 1229–1285. DOI: 10.1103/RevModPhys.81.1229.

[29] W. P. Leemans et al. "The BErkeley Lab Laser Accelerator (BELLA): A 10 GeV Laser Plasma Accelerator". In: *Particle Accelerator Conference*. 2011, pp. 1416–1420.

[30] C. G. Durfee and H. M. Milchberg. "Light pipe for high intensity laser pulses". In: *Phys Rev Lett* 71.15 (Oct. 1993), pp. 2409–2412. DOI: 10.1103/PhysRevLett.71.2409.

[31] S. M. Hooker et al. "Low Density Plasma Channels Created by Hydrodynamic Expansion of OFI-heated Plasma Columns". In: *Advanced Accelerator Concepts Workshop*. 2016.

[32] ISO11146-3. *Lasers and laser-related equipment — Test methods for laser beam widths, divergence angles and beam propagation ratios — Part 3: Intrinsic and geometrical laser beam classification, propagation and details of test methods*. 2004.

[33] J. J. MacFarlane, I. E. Golovkin and P. R. Woodruff. "HELIOS-CR – A 1-D radiation-magnetohydrodynamics code with inline atomic kinetics modeling". In: *J. Quant. Spectrosc. Radiat. Transf.* 99 (2006), pp. 381–397. DOI: 10.1016/j.jqsrt.2005.05.031.

[34] J. Fan, E. Parra and H. M. Milchberg. "Resonant self-trapping and absorption of intense Bessel beams". English. In: *Phys Rev Lett* 84.14 (2000), pp. 3085–3088. DOI: 10.1103/PhysRevLett.84.3085.

[35] T. R. Clark and H. M. Milchberg. "Optical mode structure of the plasma waveguide". English. In: *Phys Rev E* 61.2 (Feb. 2000), pp. 1954–1965. DOI: 10.1103/PhysRevE.61.1954.

[36] L. Feder, B. Miao, J. E. Shrock, A. Goffin and H. M. Milchberg. "Self-waveguiding of relativistic laser pulses in neutral gas channels". In: *Physical Review Research* 2.4 (Nov. 2020), p. 043173. DOI: 10.1103/physrevresearch.2.043173.

[37] B. Fryxell et al. "FLASH: An Adaptive Mesh Hydrodynamics Code for Modeling Astrophysical Thermonuclear Flashes". In: *The Astrophysical Journal Supplement Series* 131.1 (2008), p. 273. ISSN: 0067-0049. DOI: 10.1086/317361.

[38] A. Alejo, J. Cowley, A. Picksley, R. Walczak and S. M. Hooker. "Demonstration of kilohertz operation of hydrodynamic optical-field-ionized plasma channels". In: *Physical Review Accelerators and Beams* 25.1 (2022), p. 011301. DOI: 10.1103/physrevaccelbeams.25.011301. eprint: 2110.00448.

6 List of Symbols, Abbreviations and Acronyms

Abbreviation	Meaning
AOPDF	Acoustic-Optic Programmable Dispersive Filter
CHOFI	Conditioned Hydrodynamic Optical-Field-Ionized
CLF	Central Laser Facility, Rutherford Appleton Laboratory
EPSRC	Engineering and Physical Sciences Research Council
FEL	Free-electron laser
FWHM	Full-Width at Half-Maximum
GDD	Group Delay Dispersion
HOFI	Hydrodynamic Optical-Field-Ionized
LMU	Ludwig Maximilians Universität, Munich
LWFA	Laser Wakefield Accelerator
IP	Intellectual Property
MP-LWFA	Multi-Pulse Laser Wakefield Accelerator
P-MoPA	Plasma-Modulated Plasma Accelerator
RF	Radio-Frequency
SHG	Second Harmonic Generation
SFMI	Strong-Field Modulational Instability
TCI	Truncated-Channel Injection